An interaction between Gβγ and RNA polymerase II regulates transcription in cardiac fibroblasts

Shahriar M. Khan[†], Ryan D. Martin[†], Sarah Gora, Celia Bouazza, Jace Jones-Tabah, Andy Zhang, Sarah MacKinnon, Phan Trieu, Paul B.S. Clarke, Jason C. Tanny*, and Terence E. Hébert*

[1]Department of Pharmacology and Therapeutics, McGill University, Montréal, Québec, H3G 1Y6, Canada

†These authors contributed equally to the study.

*To whom correspondence should be addressed.

Dr. Terence E. Hébert, PhD,
Department of Pharmacology and Therapeutics,
McGill University,
3655 Promenade Sir-William-Osler, Room 1303
Montréal, Québec, H3G 1Y6, Canada
Tel: (514) 398-1398
E-mail: terence.hebert@mcgill.ca

OR

Dr. Jason C. Tanny, PhD,
Department of Pharmacology and Therapeutics,
McGill University,
3655 Promenade Sir-William-Osler, Room 1303
Montréal, Québec, H3G 1Y6, Canada
Tel: (514) 398-3608
E-mail: jason.tanny@mcgill.ca

SUMMARY

Gβγ subunits are involved in many different signalling processes in various compartments of the cell, including the nucleus. To gain insight into the functions of nuclear Gβγ, we investigated the functional role of Gβγ signalling in regulation of GPCR-mediated gene expression in primary rat neonatal cardiac fibroblasts. Following activation of the angiotensin II type I receptor in these cells, Gβγ dimers interact with RNA polymerase II (RNAPII). Our findings suggest that $G\beta_1$ recruitment to RNAPII negatively regulates the fibrotic transcriptional response, which can be overcome by strong fibrotic stimuli. The interaction between Gβγ subunits and RNAPII expands the role for Gβγ signalling in cardiac fibrosis. The Gβγ-RNAPII interaction was regulated by signaling pathways in HEK 293 cells that diverged from those operating in cardiac fibroblasts. Thus, the interaction may be a conserved feature of transcriptional regulation although such regulation may be cell-specific.

57 **INTRODUCTION**

58 In recent years, study of the role of paracrine interactions between cardiomyocytes and
59 cardiac fibroblasts in modulating the response to cardiac damage has expanded dramatically.
60 Cardiac fibroblasts, in particular, respond dynamically following damage to the myocardium
61 which is characterized by differentiation into myofibroblasts, increased proliferation and
62 migration to areas of damage (Travers et al., 2016, Fu et al., 2018, Dobaczewski et al., 2010).
63 This fibrotic response is modulated by the renin-angiotensin system, acting predominantly
64 through the peptide ligand angiotensin II (Ang II) (Murphy et al., 2015, Kawano et al., 2000).
65 Ang II drives changes in fibroblast function both directly and indirectly by increasing expression
66 of other pro-fibrotic growth factors, such as transforming growth factor β1 (TGF-β1) (Campbell
67 and Katwa, 1997). Collectively, these factors regulate alterations in cardiac architecture required
68 for tissue repair by modulating the expression of genes encoding extracellular matrix proteins
69 and proteases (Rosenkranz, 2004, Gao et al., 2009). Ang II also promotes cytokine secretion,
70 thereby triggering autocrine and paracrine signalling to elicit further responses (Cheng et al.,
71 2003, Ahmed et al., 2004). These signalling events create a feedforward loop, amplifying the
72 fibrotic response from the initial area of damage to more distal regions of the heart (Ma et al.,
73 2018). While the process initially aids in wound healing, a prolonged, activated fibrotic response
74 worsens adverse cardiac remodelling and accelerates progression to heart failure (Travers et al.,
75 2016, Weber et al., 2013). Importantly, inhibiting aspects of the fibrotic response reduces
76 adverse cardiac remodelling (Fu et al., 2018, Weber and Diez, 2016). Hence, deciphering how
77 Ang II signalling regulates pro-fibrotic gene expression is an important step towards
78 understanding how these processes might be targeted therapeutically.

79 Cardiac fibroblasts respond to increased Ang II levels through Ang II type I (AT1R) and
80 type II (AT2R) G protein-coupled receptors (GPCRs). Of these, the AT1R is responsible for
81 positively regulating the fibrotic response in cardiac fibroblasts (Travers et al., 2016). The AT1R
82 couples to multiple heterotrimeric G proteins composed of specific combinations of Gα and Gβγ
83 subunits (Namkung et al., 2018). G proteins serve as signal transducers to relay extracellular
84 ligands bound to GPCRs into activation of different intracellular signalling pathways (Khan et
85 al., 2013). Gβγ subunits, like the more extensively studied Gα subunits, modulate a wide variety
86 of canonical GPCR effectors at the cellular surface such as adenylyl cyclases, phospholipases
87 and inwardly rectifying potassium channels (Khan et al., 2013, Dupré DJ, 2009, Smrcka, 2008).
88 However, compared with Gα-mediated events, Gβγ-mediated signalling is relatively
89 understudied and is complicated by the existence of 5 Gβ and 12 Gγ subunits which can combine
90 in multiple ways to form obligate dimers. Gβγ subunits also regulate a variety of non-canonical
91 effectors in distinct intracellular locations, and a number of studies have described roles for Gβγ
92 signalling in the nucleus (Khan et al., 2013, Campden et al., 2015a). Nuclear Gβγ subunits
93 modulate gene expression through interactions with a variety of transcription factors, such as
94 adipocyte enhancer binding protein 1 (AEBP1), the AP-1 subunit c-Fos, HDAC5 and MEF2A
95 (Park et al., 1999, Robitaille et al., 2010, Spiegelberg and Hamm, 2005, Bhatnagar et al., 2013).
96 Furthermore, we have detected $G\beta_1$ occupancy at numerous gene promoters in HEK 293 cells
97 (Khan et al., 2015). While canonical Gβγ signalling has been implicated in both cardiac fibrosis
98 and heart failure (Kamal et al., 2017, Travers et al., 2017), how nuclear Gβγ signalling impacts
99 these events is currently unknown.

100 Here, we describe a novel interaction between Gβγ subunits and RNA polymerase II
101 (RNAPII) which regulates the cardiac fibrotic response to Ang II activation of AT1R. We

102 characterize the GPCR-dependent, signalling pathway-specific regulation of this interaction in
103 primary neonatal rat cardiac fibroblasts and in HEK 293 cells. To understand the potential role of
104 individual Gβγ subunits, we knocked down $G\beta_1$ and $G\beta_2$ as exemplars of Gβ subunits highly
105 expressed in these cells and characterized how nuclear $G\beta_1$, in particular, is a key regulator of
106 AT1R-driven transcriptional changes.
107
108
109
110
111
112
113
114
115
116
117
118
119
120
121
122
123
124

125

126 **RESULTS**

127 *Gβγ interaction with RNAPII following activation of Gαq-coupled GPCRs*

128 As Gβγ interacts with transcription factors and occupies gene promoter regions, we
129 hypothesized that Gβγ subunits interact with a protein complex ubiquitously involved in
130 transcription, and we initially focused on RNAPII. We assessed the potential Gβγ-RNAPII
131 interaction following endogenous M3-muscarinic acetylcholine receptors (M3-mAChRs)
132 activation with carbachol in HEK 293F cells. An initial co-immunoprecipitation time course
133 experiment revealed a carbachol-induced interaction between endogenous Gβγ subunits ($G\beta_{1\text{-}4}$
134 detected with a pan-Gβ antibody) and Rpb1, the largest subunit of RNAPII, peaking between 45
135 and 120 mins (**Supplemental Figure 1A, B**). Immunoprecipitation of Rpb1 with two different
136 antibodies also co-immunoprecipitated $G\beta_{1\text{-}4}$ in an agonist-dependent manner (**Supplemental**
137 **Figure 1C**). Further, we observed no basal or carbachol-dependent interaction of Rpb1 with
138 Gαq/11 or ERK1/2 (**Supplemental Figure 1D, E**) suggesting that Gβγ was not in complex with
139 these proteins when it was associated with RNAPII in the nucleus. Under similar conditions, we
140 observed no basal or carbachol-dependent interaction of Gβγ subunits with the A194 subunit of
141 RNA polymerase I (**Supplemental Figure 1F**), suggesting Gβγ is not recruited to all RNA
142 polymerases.

143 We next assessed the whether the Gβγ-RNAPII interaction also occurred in primary rat
144 neonatal cardiac fibroblasts following treatment with Ang II. A time-course co-
145 immunoprecipitation experiment revealed an agonist induced Gβγ-RNAPII interaction with a
146 major peak interaction observed 75 minutes post stimulation (**Figure 1A, B**). As cardiac
147 fibroblasts express both AT1R and AT2R, we next examined which receptor subtype regulated

148 the response, by pre-treatment with the AT1R-specific antagonist losartan. Pre-treatment of cells
149 with losartan prior to Ang II treatment abolished the agonist-induced interaction, but preserved
150 the basal interaction, suggesting that AT1R, and not AT2R, is primarily responsible for
151 mediating the interaction (**Figure 1C, D**).

152 Although several Gβγ isoforms have been detected in the nucleus (Bhatnagar et al., 2013,
153 Campden et al., 2015b, Zhang et al., 2001), the mechanisms leading to entry of Gβγ into the
154 nucleus remain unknown. Using subcellular fractionation following M3-mAChR activation in
155 HEK 293F cells, we observed importin-β dependent translocation of Gβγ into the nucleus **(data**
156 **not shown).** In addition, the agonist-dependent interaction of $G\beta_{1\text{-}4}$ and RNAPII was blocked by
157 importazole pre-treatment, suggesting that nuclear import of $G\beta_{1\text{-}4}$ is required for the interaction
158 with RNAPII in these cells (**Supplemental Figure 2A, B**). Next, we determined the effect of
159 importazole pre-treatment on the Ang II-mediated Gβγ-RNAPII interaction in cardiac
160 fibroblasts. The Gβγ-RNAPII interaction was also ablated when nuclear import via importin-β
161 was inhibited, suggesting again that Gβγ subunits must translocate to the nucleus for the
162 interaction with RNAPII to occur (**Figure 1E, F**).

163

164 *Signalling pathways regulating Gβγ-RNAPII interaction are cell-specific*

165 We next examined signalling events downstream of receptor activation that could
166 mediate the interaction between Gβγ subunits and RNAPII. To this end, we pursued a
167 pharmacological and genetic approach using both cardiac fibroblasts (**Figure 2**) and HEK 293F
168 cells (**Figure 3)**. Our data indicated that the pathways responsible for promoting the Gβγ-
169 RNAPII interaction are cell type specific. Since AT1R couples to both Gq/11 and Gi/o G
170 proteins (Sauliere et al., 2012), we used FR900359 to inhibit Gαq/11 (Schrage et al., 2015) and

171 pertussis toxin (PTX) to inhibit Gαi/o. The agonist-induced response was markedly (~80%)
172 decreased by the Gαq/11 inhibitor, and also decreased (~30%) by the Gαi/o inhibitor,
173 demonstrating that AT1R signalling through Gαq is the primary pathway leading to increased
174 Gβγ-RNAPII interaction (**Figure 2A-B, Supplemental Figure 3A-B**). We next used U71322 to
175 inhibit the activity of phospholipase Cβ (PLCβ), downstream of both Gq/11 and Gi/o (the latter
176 via Gβγ signalling). In cardiac fibroblasts, pre-treatment of U71322 blocked the agonist-induced
177 Gβγ-RNAPII interaction with no effect on the basal interaction, suggesting a pivotal role for
178 PLCβ (**Figure 2C, Supplemental Figure 3C**). Chelation of Ca^{2+} using BAPTA-AM in cardiac
179 fibroblasts also abrogated the Ang II-induced Gβγ-RNAPII interaction (**Figure 2D,**
180 **Supplemental Figure 3D**), as did treatment with the PKC inhibitor Gö6983 and the CaMKII
181 inhibitor KN-93 (**Figure 2E, F, Supplemental Figure 3E, F**). Conversely, the MEK1 inhibitor
182 U0126 led to an increased basal Gβγ-RNAPII interaction but abrogated the Ang II-induced
183 interaction (**Figure 2G, Supplemental Figure 3G**). Lastly, the calcineurin inhibitor cyclosporin
184 A lead to an increased basal interaction did not prevent further Ang II-dependent increase in
185 interaction (**Figure 2H**, **Supplemental Figure 3H**).

186 Extending these studies to HEK 293F cells, we observed a similar reliance on Gαq
187 signalling for the agonist-induced Gβγ-RNAPII interaction. The carbachol-induced Gβγ-RNAPII
188 interaction was prevented by pre-treatment with the Gαq inhibitor FR900359 (**Figure 3A and**
189 **Supplemental Figure 4A**) and also by CRISPR/Cas9-mediated knockout of Gαq/11/12/13
190 (**Figure 3B and Supplemental Figure 4B**). However, except for this common event, the
191 signalling pathways in cardiac fibroblasts and HEK 293F cells diverged substantially. In HEK
192 293F cells, U71322 also blocked the carbachol-induced Gβγ-RNAPII interaction but there was a
193 pronounced increase in the basal interaction (**Figure 3C, Supplemental Figure 4C**). Further

194 differences were observed following chelation of calcium with BAPTA-AM which increased
195 basal levels of the Gβγ-RNAPII interaction but did not block further carbachol-induced
196 stimulation of the interaction (**Figure 3D, Supplemental Figure 4D**), suggesting a modulatory
197 role for calcium in HEK 293F cells rather than the direct role seen in cardiac fibroblasts. HEK
198 293F cells employed different regulatory mechanisms involving protein kinases activated
199 downstream of Gαq/11-coupled GPCRs compared to cardiac fibroblasts. For example, the PKC
200 inhibitor Gö6983 and the CaMKII inhibitor KN-93 both increased basal levels of interaction but
201 did not block carbachol-induced interactions between Gβγ and Rpb1 (**Figure 3E, F,**
202 **Supplemental Figure 4E, F**). Indeed, inhibition of calcineurin with cyclosporin A blocked the
203 carbachol-mediated increase in interaction between Gβγ and Rpb1, suggesting a role for this
204 phosphatase in mediating the interaction in response to M3-mAChR activation (**Figure 3G** and
205 **Supplemental Figure 4G**). While the requirement for activation of Gαq is common for the Gβγ-
206 RNAPII interaction in both cell types, the regulation by downstream signalling pathways
207 diverges.
208
209 *Roles of individual Gβ subunits in regulating the angiotensin II-activated fibrotic response in rat*
210 *neonatal cardiac fibroblasts*
211 The Gβ family is comprised of five members which, with the exception of $G\beta_5$, exhibit
212 high levels of sequence and structural similarity (Khan et al., 2013). Despite these similarities,
213 Gβ isoforms differ considerably with respect to their associated receptors and signalling
214 pathways (Khan et al., 2015, Yim et al., 2019, Greenwood and Stott, 2019). As our above-
215 reported characterization used a pan-$G\beta_{1\text{-}4}$ antibody, we next sought to examine the specificity of
216 Gβ isoforms interacting with Rpb1 in cardiac fibroblasts. We initially focused on $G\beta_1$ and $G\beta_2$ as

217 they exhibit the highest expression in cardiac fibroblasts determined by RNA-seq (Shu et al.,
218 2018) and RT-qPCR (**Supplemental Figure 5A**). Immunoprecipitation with a $G\beta_1$ specific
219 antibody revealed an increase in the amount of Rpb1 co-immunoprecipitated in response to Ang
220 II treatment, whereas immunoprecipitation of $G\beta_2$ indicated a basal interaction with Rpb1 that
221 was lost in response to Ang II treatment (**Supplemental Figure 5B**). We also assessed Gβ
222 isoform specificity in HEK 293F cells through heterologous expression of FLAG-tagged
223 versions of each Gβ subunit. In response to M3-mAChR activation, FLAG-$G\beta_1$ was the only
224 isoform that showed an increased interaction with Rpb1 (**Supplemental Figure 5C, D**). Hence,
225 an increased interaction between $G\beta_1$ and Rpb1 was seen in both cell types, suggesting that our
226 earlier observations using the pan-$G\beta_{1\text{-}4}$ antibody likely reflected increased interactions with $G\beta_1$.
227 As we observed isoform-specific roles in RNAPII interactions, we next assessed how
228 knockdown of either Gβ isoform affected the interaction. We first validated knockdown
229 conditions for each Gβ subunit by siRNA at the mRNA and protein levels (**Supplemental**
230 **Figure 6A, B**). We observed a reduction in the Ang II-induced Gβγ-RNAPII interaction upon
231 knockdown of $G\beta_1$, supporting $G\beta_1$ as the isoform involved in the increased interaction with
232 Rpb1. Surprisingly, knockdown of $G\beta_2$ also prevented the Ang II-mediated increase in the Gβγ-
233 RNAPII interaction (**Figure 4A, B)**. The loss of Gβγ-RNAPII interaction after $G\beta_2$ knockdown,
234 despite it not being involved in the Ang II-dependent increase, suggested that AT1R signalling
235 could be altered by loss of $G\beta_2$ subunits.
236 We thus determined whether specific Gβ isoforms were required to initiate signalling
237 cascades proximal to AT1R activation. Following receptor activation, Gβγ subunits regulate
238 intracellular Ca^{2+} mobilization through activation of PLCβ (Park et al., 1993). As we have
239 previously demonstrated Gβ isoform specificity for PLCβ signalling in HEK 293F cells (Khan et

240 al., 2015), we assessed the relative roles of $G\beta_1$ and $G\beta_2$ in AT1R-dependent Ca^{2+} mobilization.
241 To assess AT1R-dependent intracellular Ca^{2+} mobilization, we used the cell-permeable Ca^{2+} dye
242 Fura 2-AM. Following AT1R activation, we observed a rapid increase in intracellular Ca^{2+}
243 mobilization (**Figure 4A**, black, empty triangles) and the quantified area under the curve (**Figure**
244 **4B**, black bar). Knockdown of $G\beta_1$ did not alter Ca^{2+} mobilization following stimulation with
245 Ang II (8.1 ± 7.0% decrease, red bar). However, knockdown of $G\beta_2$ resulted in a significant 31.6
246 ± 9% decrease in Ca^{2+} release (**Figure 4A, B**, green bar), suggesting a role for $G\beta_2$-containing
247 Gβγ dimers in mediating receptor-proximal signalling downstream of AT1R activation. This
248 suggests Gβ2 knockdown prevented the Ang II-dependent increase in Gβγ-RNAPII interaction
249 through disruption to AT1R Ca^{2+} signalling, aligning with the observed effect of Ca^{2+} chelation
250 with BAPTA-AM. These results highlight the complex interplay between cell surface receptors
251 and multiple Gβγ subunits, in modulating both basal and ligand stimulated RNAPII/Gβγ
252 interactions.
253
254 *Gβγ interacts with transcribing RNAPII*
255 As we demonstrated that Gβγ is recruited to RNAPII following AT1R activation, which
256 also activates a transcriptional program in fibroblasts, we assessed the relationship between the
257 transcriptional response and Gβγ recruitment (Shu et al., 2018, Dang et al., 2015). To assess this
258 potential relationship, we disrupted the transcription cycle at two different regulatory points
259 through inhibition of Cdk7, a component of the general transcription factor TFIIH, and Cdk9, the
260 protein kinase subunit of P-TEFb (Zhou et al., 2012). Following RNAPII recruitment, Cdk7
261 activity stimulates promoter clearance of RNAPII to begin transcription. Soon after RNAPII
262 pauses at a promoter-proximal region and requires the activity of Cdk9 in order to be released

263 into productive elongation (Liu et al., 2015). We assessed involvement of both Cdk7 and Cdk9
264 on the Ang II-induced Gβγ-RNAPII interaction using the selective inhibitors THZ1 and iCdk9,
265 respectively (Lu et al., 2015, Kwiatkowski et al., 2014). THZ1 abrogated the Ang II-stimulated
266 Gβγ-RNAPII interaction (**Figure 5A, Supplemental Figure 7A**) while iCdk9 resulted in a loss
267 of both the basal and Ang II-stimulated Gβγ-RNAPII interaction (**Figure 5B, Supplemental**
268 **Figure 7B**). This suggests that the Gβγ-RNAPII interaction requires the transcriptional response
269 to Ang II in cardiac fibroblasts. As with cardiac fibroblasts, in HEK 293F cells disruption of the
270 transcriptional cycle through inhibition of Cdk7 and Cdk9 with DRB also blocked the increased
271 interaction between RNAPII and Gβγ (**data not shown**), showing that the Gβγ/RNAPII
272 interaction is dependent on an active transcriptional response in both cell types.
273
274 *The role of Gβγ subunits in fibrotic gene expression*
275 In order to understand the role of Gβγ in Ang II-regulated gene expression, we examined
276 changes in the levels of 84 genes involved in the fibrotic response using the Qiagen RT^2
277 Profiler™ PCR array platform. Gene expression changes were assessed following 75 min or 24 h
278 Ang II treatment alongside Gβ1 or Gβ2 knockdown. These two time points were selected to
279 investigate the effect of disrupting the Gβγ-RNAPII interaction or, in the longer term, upstream
280 signalling, respectively. We assessed gene expression changes across all 67 genes remaining
281 after excluding genes below our chosen threshold of detection (i.e. Ct > 35). After 75 min of Ang
282 II treatment, we observed a similar upregulation of fibrotic genes in both control and $G\beta_1$
283 knockdown conditions (**Figure 5C, Supplemental Table 1**). However, $G\beta_1$ knockdown
284 increased both basal expression and the total number of genes altered by AT1R stimulation
285 (**Figure 5C, Supplemental Table 1**). Following 24 h Ang II treatment, this effect became more

286 pronounced. $G\beta_1$ knockdown led to increases in basal gene expression, expression regulated by
287 Ang II treatment and the overall number of genes upregulated (**Figure 5D, Supplemental Table**
288 **1**). The increased expression following $G\beta_1$ knockdown suggests the Gβγ-RNAPII interaction
289 negatively modulates the Ang II transcriptional response.

290 Whereas Gβ1 knockdown altered the transcriptional response to Ang II treatment,
291 disruption of AT1R signalling by $G\beta_2$ knockdown did not significantly alter basal fibrotic gene
292 expression or the overall response to 24 h Ang II treatment (**Figure 5D, Supplemental Table 1**).
293 The lack of effect of $G\beta_2$ knockdown suggests that Gβγ signalling through Ca^{2+} is not required
294 for AT1R-mediated transcriptional changes. To further address the role of Gβγ signalling, we
295 utilized the small-molecule pan-Gβγ inhibitor gallein (Lehmann et al., 2008). As with $G\beta_2$
296 knockdown, pre-treatment with gallein did not significantly alter the transcriptional response
297 following 24 h Ang II treatment (**Figure 5E**). This suggests that Gβγ-dependent signalling
298 downstream of the AT1R is not a key driver of transcriptional changes. Instead, Gβγ is required
299 to modulate processes driven by other signalling pathways and dampen the fibrotic response
300 until such signals rise above a threshold.

301

302 *Genome-wide recruitment of $G\beta_1$ and the effect on RNAPII occupancy following Ang II*
303 *treatment*

304 To assess the possibility of genome-wide $G\beta_1$ recruitment and changes in RNAPII
305 occupancy following 75 min Ang II treatment in cardiac fibroblasts, we performed chromatin
306 immunoprecipitation followed by next generation sequencing (ChIP-seq) for heterologously
307 expressed FLAG-$G\beta_1$ and endogenous Rpb1. We confirmed that, like endogenous $G\beta_1$, the
308 interaction of Rbp1 with heterologously expressed FLAG-$G\beta_1$ increased following AT1R

309 activation (**Supplemental Figure 8A, B**). We focused on genes with RNAPII peaks identified by
310 the peak calling software macs2 and annotated with HOMER (Heinz et al., 2010, Zhang et al.,
311 2008). The same $G\beta_1$ knockdown conditions that increased the number of genes upregulated in
312 response to Ang II (above) also increased the number of genes occupied by RNAPII following
313 Ang II treatment (**Figure 6A**). To identify groups of genes with similar FLAG-$G\beta_1$ and RNAPII
314 occupancy patterns, we performed K-means clustering with genes that RNAPII peaks were
315 identified in any treatment condition. Two K-means clusters were identified (98 genes in cluster
316 1 and 806 in cluster 2) with distinct occupancy patterns (**Figure 6B, C**). In cluster 1, FLAG-$G\beta_1$
317 occupancy increased within the gene body in response to Ang II. A similar but weaker tendency
318 was also observed in cluster 2 (**Figure 6B**). The increased FLAG-Gβ1 occupancy in cluster 1
319 corresponded to Gβ1-dependent changes to the Ang II-induced RNAPII occupancy alterations.
320 First, Ang II treatment led to increased RNAPII occupancy throughout the gene body under
321 siRNA control conditions (**Figure 6C**). In the absence of Ang II, $G\beta_1$ knockdown increased
322 RNAPII occupancy near transcription start sites (TSSs) which corresponds with increased gene
323 expression under these conditions (**Figure 6C**). Lastly, there was greater RNAPII occupancy
324 when Ang II treatment was combined with Gβ1 knockdown than in the absence of knockdown
325 (**Figure 6C**). Similar RNAPII occupancy patterns were observed in cluster 2, suggesting that
326 Gβ1 also plays a regulatory role along these genes and our FLAG-$G\beta_1$ ChIP-seq was not
327 sensitive enough to reliably detect $G\beta_1$. We also assessed the functional pathways enriched in
328 cluster 1, through gene ontology (GO) term enrichment. The top four significant GO terms
329 identified (corresponding to cellular processes such as inflammation, fibroblast activation and
330 apoptosis) indicate that $G\beta_1$ is recruited to genes involved in processes essential to fibrosis
331 (**Figure 6D**).

332 The increased number of genes with RNAPII occupancy in the Ang II and Gβ1
333 knockdown condition suggested that $G\beta_1$ occupancy impairs RNAPII recruitment. As such, we
334 would expect cluster 1 genes to be more enriched in genes with RNAPII occupancy under Ang II
335 and Gβ1 knockdown condition than Ang II and siRNA control conditions. Therefore, we
336 performed a Fisher's exact test to compare the proportion of cluster 1 genes in these treatment
337 conditions, which demonstrated a significant (p-value < 0.01) enrichment in the Ang II and Gβ1
338 knockdown condition gene list compared to Ang II and siRNA control condition. This again
339 suggests $G\beta_1$ functions to suppress RNAPII transcription following AT1R activation.

340 In order to assess the relationship between $G\beta_1$ occupancy and transcription, we focused
341 on genes from our fibrosis qPCR array that were also found in cluster 1. Eight genes from the
342 fibrosis array were identified in cluster 1, which included five of the seven genes upregulated
343 after 75 min of Ang II treatment such as thrombospondin 1 (Thbs1) and connective tissue growth
344 factor (Ctgf) (**Figure 6E, F**). We confirmed the Ang II-dependent increase in $G\beta_1$ occupancy
345 along Ctgf by ChIP-qPCR (**Supplemental Figure 8C**). We also assessed the effect of $G\beta_1$
346 knockdown on AT1R-dependent changes of RNAPII occupancy along Ctgf by ChIP-qPCR.
347 Similar to our ChIP-seq analysis, we observed a greater increase in RNAPII along the gene in
348 response to Ang II under siRNA GNB1 knockdown compared to siRNA control, where we
349 observed a slight decrease (**Supplemental Figure 8D**). We also validated the change in
350 expression of Ctgf by RT-qPCR using primers designed in-house (**Supplemental Table 2**).
351 Under control conditions Ang II had a minor effect on Ctgf expression, however in the absence
352 of $G\beta_1$ Ang II treatment resulted in a significant upregulation of Ctgf mRNA. (**Supplemental**
353 **Figure 8E**). Taken together, our results demonstrate $G\beta_1$ recruitment negatively regulates

354 expression of genes involved in the fibrotic response to Ang II by inhibiting early stages of the
355 RNAPII transcription cycle.
356
357
358
359
360

361 **DISCUSSION**

362 The functional specificity of Gβ and Gγ subunits has been mostly investigated in the
363 context of signalling proximal to GPCR activation (i.e., the regulation of effector activity
364 downstream of receptor stimulation) (Khan et al., 2013). In contrast, our findings provide new
365 insights regarding non-canonical roles of specific Gβγ dimers in more distal events in the
366 nucleus, particularly in the regulation of gene expression. Here, we demonstrate for the first time
367 an interaction between Gβγ and RNAPII and investigate the regulatory signalling mechanisms in
368 transformed cell lines (HEK 293 cells) and in primary cells (neonatal rat cardiac fibroblasts). The
369 interaction of Gβγ and RNAPII represents a significant addition to the expanding list of Gβγ
370 interactors, and our findings suggest that regulatory mechanisms impacting the interaction are
371 dependent on cellular context. We also show that Gβγ signalling is a critical regulator of the
372 fibrotic response in cardiac fibroblasts.

373 Our findings suggest that following acute treatment with Ang II, $G\beta_1$ is transiently
374 recruited to pro-fibrotic genes to negatively regulate RNAPII recruitment, thereby limiting the
375 fibrotic response following transient fluctuations in local Ang II concentrations likely seen *in*
376 *vivo*. This negative RNAPII regulation may potentially occur through direct interactions with
377 RNAPII, preventing its recruitment or other aspects of initiation, or else via an indirect
378 mechanism in which Gβγ would form part of a larger RNAPII-containing complex altering the
379 local chromatin landscape. We cannot currently distinguish between these two possibilities,
380 given that our co-immunoprecipitation assay was performed using whole-cell lysates. On the
381 other hand, chronic stress or damage to the heart leads to a sustained increase of Ang II
382 concentrations in cardiac tissue (Sun and Weber, 1996, Passier et al., 1996). We propose that
383 such sustained AT1R signalling overcomes the transient $G\beta_1$ "brake" to elicit a robust fibrotic

384 response. Alternatively, pro-fibrotic factors that are upregulated and secreted following AT1R
385 activation may elicit autocrine signalling pathways that overcome the $G\beta_1$ transcriptional
386 repression (Lee et al., 1995, Ma et al., 2018). Our gene expression data at 75 min, and more
387 especially at 24 h, begins to identify the increased number and greater gene expression in the
388 absence of the proposed negative regulatory mechanism when $G\beta_1$ is knocked down. Further
389 analysis of the kinetics of the interaction and how this changes the dynamics of chromatin
390 occupation or gene expression are required as well. Future experiments assessing nascent RNA
391 production are required to accurately determine gene expression changes at early time points.

392 We demonstrated that $G\beta_2$, and not $G\beta_1$, was important for proximal signalling
393 downstream of AT1R activation similar to the requirement of specific Gβ isoforms for activation
394 of PLCβ in HEK 293 cells (Khan et al., 2015). Our data suggest that $G\beta_2$ plays a minimal role in
395 regulating AT1R-dependent gene expression *per se*. Rather, our findings using the broad-
396 spectrum Gβγ inhibitor gallein suggest that receptor-proximal Gβγ signalling in general is not
397 required for the transcriptional response and instead it is dependent on Gαq signalling and more
398 distal $G\beta_1$-dependent events. Knockdown of $G\beta_2$ also compromised Ang II-mediated interactions
399 between Gβγ and RNAPII even though $G\beta_2$ had a limited role in the fibrotic transcriptional
400 response. This suggests $G\beta_2$ knockdown does not prevent the response but rather alters the
401 kinetics of Gβγ-RNAPII interactions, which then translates into different fibrotic responses over
402 time. Further, the roles of specific Gγ subunits in mediating proximal signal transduction must
403 also be considered as for other Gβγ effectors (Khan et al., 2015), and should be the subject of
404 future studies. Taken together, our findings suggest that in fibrosis and potentially in other
405 diseases, the indiscriminate targeting of Gβγ signalling (e.g. with compounds such as gallein)

406 will result in outcomes that differ considerably from those obtained by targeting particular Gβγ
407 combinations (Lin and Smrcka, 2011, Kamal et al., 2011, Smrcka et al., 2008).

408 Analysis of the signalling networks regulating the Gβγ/RNAPII interaction yielded four
409 main conclusions: (1) different GPCR signalling systems in distinct cell types lead to different
410 kinetics of the Gβγ-RNAPII interaction, (2) different signalling pathways downstream of GPCR
411 activation act to both induce or modulate the interaction, (3) Gαq-coupled GPCRs regulate the
412 interaction in both cell types examined, and (4) signalling ultimately converged on activation of
413 transcription. Indeed, our results suggest that the cell context plays a critical role in determining
414 the mechanism by which the Gβγ-RNAPII interaction is regulated. First, in cardiac fibroblasts,
415 the Gβγ/RNAPII interaction depended on a Gq-PLCβ-Ca^{2+}-CaMKII/PKC/MEK-dependent
416 pathway downstream of AT1R activation, whereas calcineurin acted as a basal negative regulator
417 (summarized in **Supplemental Figure 9**). On the other hand, in HEK 293 cells, we observed that
418 the interaction was reliant on a Gq-PLCβ-Ca^{2+}-calcineurin pathway downstream of M3-mAChR
419 activation, whereby PKC and CaMKII both negatively regulate this interaction under basal
420 conditions (summarized in **Supplemental Figure 9**). The involvement of Ca^{2+}, PKC and
421 ERK1/2 in the induction of the Gβγ/RNAPII interaction in fibroblasts is supported by previous
422 reports that demonstrate their involvement in Ang II-induced fibrosis (Chintalgattu and Katwa,
423 2009, Olson et al., 2008).

424 The different signalling pathways promoting the Gβγ-RNAPII interaction appear to
425 converge at the point of Cdk7 and Cdk9 activation. In particular, we found that the Cdk7 and
426 Cdk9 inhibitors (DRB, THZ1 and iCdk9, respectively) inhibited both carbachol-induced Gβγ-
427 RNAPII interaction in HEK 293 cells and the analogous Ang II-induced interaction in cardiac
428 fibroblasts. This suggests the differential regulatory signalling pathways identified are due to cell

429 type- and receptor-specific activation pathways of both Cdk7 and Cdk9. The recruitment of Gβγ
430 serves as a common negative regulatory mechanism regardless of the pathway leading to
431 transcriptional activation. Furthermore, a strong connection has been established between the
432 control of transcriptional pausing and pathological cardiac remodelling, although primarily in the
433 cardiomyocyte (Yang et al., 2017, Sayed et al., 2013, Anand et al., 2013, Duan et al., 2017,
434 Stratton et al., 2016, Sano et al., 2002). Our results indicate that regulation of the early stages of
435 the RNAPII transcription cycle is also an important checkpoint in the fibrotic response mediated
436 by cardiac fibroblasts.

437 Taken together, the Gβγ-RNAPII interaction identifies a new mechanism by which Gβγ
438 modulates gene expression. Our study highlights the complex interplay of different Gβγ subunit
439 combinations at the cell surface and in the nucleus initiated upon stimulation of Gαq-coupled
440 receptors. Since $G\beta_1\gamma$ dimers play an important role in regulating the expression of fibrotic genes
441 in cardiac fibroblasts, the development of selective $G\beta_1\gamma$ inhibitors hold some promise for
442 preventing the pathological consequences of myocardial damage.
443
444
445
446
447
448
449
450
451

452 **METHODS**

453

454 **Reagents** –The following were all purchased from Sigma-Aldrich: carbachol, angiotensin II,
455 BAPTA-AM, KN-93, Gö6983, PTX, U0126, calyculin A, cyclosporin A, TRI reagent, isopropyl
456 thiogalactopyranoside (IPTG), protease inhibitor cocktail, triton X-100, bovine serum albumin,
457 ethylenediaminetetraacetic acid (EDTA), 70% NP-40 (Tergitol), sodium deoxycholate,
458 magnesium chloride, lithium chloride, anti-rabbit IgG (whole molecule)-agarose antibody, anti-
459 mouse IgG (whole molecule)-agarose antibody, goat anti-rabbit IgG (whole molecule)
460 conjugated to peroxidase secondary antibody, goat anti-mouse IgG (Fab specific) conjugated to
461 peroxidase secondary antibody, anti-FLAG M2 antibody, and rabbit IgG (St. Louis, MO, USA).
462 U71322 pan-PKC inhibitor was purchased from Biomol International (Plymouth Meeting, PA,
463 USA). Lysozyme (from hen egg white) and phenylmethylsulfonyl fluoride (PMSF) were
464 purchased from Roche Applied Sciences (Laval, QC, Canada). Ethylene glycol bis (2-
465 aminooethyl ether) N,N,N',N' tetraacetic acid (EGTA) and HEPES were purchased from
466 BioShop (Burlington, ON, Canada). Sodium chloride, glutathione (reduced form), dithiothreitol
467 (DTT) and Dynabeads protein G were purchased from Fisher Scientific (Ottawa, ON, Canada).
468 Dulbecco's modified Eagle's medium (DMEM) (supplemented with 4.5 g/L glucose, L-glutamine
469 and phenol red), DMEM low glucose (supplemented with 1.0 g/L glucose, L-glutamine and
470 phenol red), Hank's Balanced salt solution (HBSS), HBSS (with no phenol),
471 Penicillin/Streptomycin solution, Tris base buffer, ampicillin sodium salt, and fetal bovine serum
472 were purchased from Wisent (St. Bruno, QC, Canada). Glutathione sepharose 4B GST beads was
473 purchased from GE Healthcare (Mississauga, ON, Canada). Lipofectamine 2000 and Alexa Fluor
474 488 goat anti-mouse IgG were purchased from Invitrogen (Burlington, ON, Canada). Enhanced

475 chemiluminescence (ECL) Plus reagent was purchased from Perkin Elmer (Woodbridge, ON,
476 Canada). Moloney murine leukemia virus reverse transcriptase (MMLV-RT) enzyme and
477 recombinant RNasin® ribonuclease inhibitor were purchased from Promega (Madison, WI,
478 USA). Evagreen 2X qPCR MasterMix was purchased from Applied Biological Materials Inc.
479 (Vancouver, BC, Canada) and iQ SYBR Green Supermix was purchased from Bio-Rad
480 Laboratories (Mississauga, ON, Canada). Anti-Gβ1-4 (T-20) antibody, anti-RNA Polymerase I
481 Rpa194 (N-16) antibody, anti-ERK1/2 antibody, anti-Gαq antibody and anti-Rpb1 (N20) were
482 purchased from Santa Cruz Biotechnology, Inc. (Dallas, TX, USA). Anti-RNA polymerase II
483 clone CTD4H8 (Rpb1) antibody was purchased from EMD Millipore (Temecula, CA, USA).
484 Anti-*Schizosaccharomyces pombe* histone H2B (ab188271) antibody was purchased from
485 Abcam Inc. (Toronto, ON, Canada). Polyclonal anti-$G\beta_1$ and anti-$G\beta_2$ were a generous gift of
486 Professor Ron Taussig (UT Southwestern). THZ1 was a gift from Nathanael S. Gray (Harvard
487 University) and iCdk9 was a gift from James Sutton (Novartis). FLAG-$G\beta_1$, FLAG-$G\beta_2$, FLAG-
488 $G\beta_3$, FLAG-$G\beta_4$ and FLAG-$G\beta_5$ plasmids were obtained from UMR cDNA Resource
489 (www.cdna.org).
490
491 **Tissue culture, transfection and treatments** – Human embryonic kidney 293 (HEK 293), HEK
492 293T cells and CRISPR/Cas9 generated ΔGαq/11/12/13 knockout HEK 293 cells (quadKO cells)
493 (Devost et al., 2017), a generous gift from Dr. Asuka Inoue (Tohuku University, Sendai, Japan),
494 were grown at 37°C in 5% CO_2 in DMEM supplemented with 5% (v/v) fetal bovine serum and
495 1% (v/v) penicillin/streptomycin (P/S). HEK 293 cells were transiently transfected with FLAG-
496 Gβ1-5 using Lipofectamine 2000 as per the manufacturer's recommendations. Primary rat
497 neonatal cardiac fibroblasts were isolated from 1-3 day old Sprague-Dawley rat pups (Charles

498 River Laboratories, St-Constant, Quebec) as previously described (Calderone et al., 1998). All
499 procedures using animals were approved by the McGill University Animal Care Committee, in
500 accordance with Canadian Council on Animal Care Guidelines. Two days after isolation, cells
501 were detached with trypsin/EDTA and plated at a density of ~8 x 10^3 cells/cm^2 in fibroblast
502 growth medium for 48h. For siRNA transfection, cardiac fibroblasts were plated at a density of
503 ~20 x 10^3 cells/cm^2 and transfected using Lipofectamine 2000 as per the manufacturer's
504 instructions. For treatment of HEK 293F cells, HEK 293F quadKO cells or cardiac fibroblasts,
505 cells were serum-deprived for 6 h with DMEM or overnight (~12 h) with DMEM low glucose
506 (with no FBS and no P/S) respectively, and subsequently treated with pathway inhibitors, 1 mM
507 carbachol or 1 μM Ang II for the treatment lengths indicated in the various assays.
508
509 **RT-qPCR** – Reverse transcription of RNA isolated from rat neonatal cardiac fibroblasts was
510 performed as previously described (Khan et al., 2015). Briefly, cells were lysed in TRI reagent
511 and RNA was extracted using a protocol adapted from Ambion (Burlington, ON, Canada).
512 Reverse transcription was performed on 1 μg of total RNA using an MMLV-RT platform
513 according to the manufacturer's protocol. Subsequent qPCR analysis was performed with
514 Evagreen Dye qPCR master-mixes using a Corbett Rotorgene 6000 thermocycler or Bio-Rad
515 1000 Series Thermal Cycling CFX96 Optical Reaction module. mRNA expression data were
516 normalized to housekeeping transcripts for U6 snRNA. Ct values obtained were analyzed to
517 calculate fold change over respective control values using the $2^{-\Delta\Delta Ct}$ method. Primer sequences
518 for all primers used are listed in **Supplemental Table 2**.
519

520 **Ca^{2+} mobilization** – Cardiac fibroblasts were cultured as previously described following
521 transfection with respective siRNA. Cardiac fibroblasts were washed and media replaced with
522 HBSS (no phenol) and incubated for 1 h at 37°C and 5% CO_2. Media was replaced with Fura 2-
523 AM in HBSS and incubated for another 1 h at 37°C and 5% CO_2. Fura 2-AM containing media
524 was replaced with HBSS and Cardiac fibroblasts incubated for another 30 min at 37°C and 5%
525 CO_2 prior to recordings. Baseline recordings were obtained every 0.7 s for 10 s followed by
526 injection of Ang II to a final concentration of 1 μM and recordings obtained every 0.7 s for a
527 total of 1 min. A control well with no Fura-2 AM was included in order to control for
528 background fluorescence. Fluorescence intensity was recorded using Bio-Tek Synergy 2 Multi-
529 Mode Microplate Reader with fluorescence excitation at 340 nm or 360 nm and fluorescence
530 emission at 516 nm. Data is presented as the ratio of fluorescence emission at 516 nm following
531 340 nm excitation over 360 nm excitation. The ratio was normalized to the mean baseline ratio
532 from control cells.
533
534 **Nuclear isolation** – Nuclei from HEK 293 cells and cardiac fibroblasts were isolated as
535 previously described (Campden et al., 2015b). Briefly, cells seeded in T175 flasks (Corning)
536 were treated as indicated, washed three times with 1X PBS (137 mM NaCl, 2.7 mM KCl, 10 mM
537 Na_2HPO_4, 1.8 mM KH_2PO_4), and harvested in 1X PBS by centrifugation. Pelleted cells were
538 lysed in lysis buffer (320mM sucrose, 10 mM HEPES, 5 mM $MgCl_2$, 1 mM DTT, 1 mM PMSF,
539 1% Triton X-100), added gently on top of a high-sucrose buffer (1.8 M sucrose, 10 mM HEPES,
540 5 mM $MgCl_2$, 1 mM DTT, 1 mM PMSF), and centrifuged at 4600 g for 30 min at 4°C,
541 separating unlysed nuclei from the cytosolic fraction. Pelleted nuclei were then resuspended in

542 resuspension buffer (320 mM sucrose, 10 mM HEPES, 5 mM $MgCl_2$, 1 mM DTT, 1 mM
543 PMSF), pelleted at 300 g for 5 min and subsequently lysed in 1X RIPA buffer.
544
545 **Immunoprecipitation and western blotting** – Immunoprecipitation (IP) assays of Gβ and Rpb1
546 pull downs were performed as previously described, with minor alterations (Robitaille et al.,
547 2010). Protein extracts from treated HEK 293 cells and cardiac fibroblasts lysed in RIPA (1%
548 NP-40, 50 mM Tris-HCl ph 7.4, 150 mM NaCl, 1 mM EDTA, 1 mM EGTA, 0.1% SDS, 0.5%
549 sodium deoxycholate) were quantified by Bradford assay and 500 μg of protein lysate was
550 precleared with 15 μl of anti-rabbit IgG-agarose beads. Precleared lysates were then incubated
551 with 1 μg anti-$G\beta_{1-4}$, 2 μg of anti-Rpb1 or anti-$G\beta_1$ serum or anti-$G\beta_2$ serum overnight at 4°C
552 with end-over mixing. The next day, 40 μl of washed agarose beads were added to each
553 lysate/antibody mixture, incubated for 3.5 hours at 4°C with end-over mixing, and then beads
554 were washed 3X with RIPA. Proteins were eluted off the beads by the addition of 4X Laemmli
555 buffer followed by denaturation at 65°C for 15 min. Protein immunoprecipitation and co-IP were
556 then assessed by western blot as previously described (Khan et al., 2015). Resulting western blot
557 images were quantified using ImageJ 1.48v.
558
559 **Rat Fibrosis qPCR arrays –** Fibrosis qPCR arrays were performed as per the manufacturer's
560 instructions (Qiagen, Toronto, ON, Canada). Briefly, 0.5 μg of isolated total RNA from siRNA
561 transfected and vehicle or Ang II treated cardiac fibroblasts was subject to genomic DNA
562 elimination using mixes supplied with the array kit for 5 mins at 42°C. DNA eliminated RNA
563 was then subject to reverse transcription reactions using Qiagen RT^2 First Strand Kits with
564 protocols according to the manufacturer's instructions. Qiagen RT^2 SYBR Green MasterMix was

565 added to the cDNA and subsequently dispensed in wells of a 96-well plate containing pre-loaded
566 lyophilized primers provided by the manufacturer. Quantitative PCR reactions were then run on
567 an Applied Biosystems ViiA 7 thermocycler according to the manufacturers cycle
568 recommendations. Each sample was run on separate individual 96 well plates and Ct values for
569 each gene assessed were collected and analyzed; Ct values greater than 35 were eliminated from
570 the overall analysis. Expression data was normalized to levels of two housekeeping genes
571 contained on each plate – Ldha1 and Hprt.
572
573 **AAV Production and transduction of cardiac fibroblasts –** FLAG-Gβ_1 and FLAG-Gβ_2 were
574 PCR amplified from a pcDNA3.1+ plasmid and BamHI and EcoRI restrictions sites added to the
575 5' and 3' end, respectively. These restrictions sites were used to insert each FLAG-Gβ into the
576 pAAV-CAG plasmid. Adeno-associated viruses were produced as previously described (Burger
577 and Nash, 2016). Cells were transduced with AAV1-FLAG-Gβ_1 (MOI of 10^3 or $5x10^4$) in
578 DMEM low glucose for 6h. Additional media was added to obtain a final 7% FBS concentration
579 and incubated for another 24 h. At this point, the cells were detached with trypsin/EDTA and
580 plated as described for respective experiments.
581
582 **ChIP-qPCR –** Immunoprecipitation in cardiac fibroblasts was performed as previously
583 described, with minor modifications (Bolli et al., 2013). Isolated nuclei were sonicated with a
584 Diagenode BioRuptor™ UCD-200 (18 cycles, 30 s on/off, high power) to shear chromatin.
585 FLAG-Gβ_1 immunoprecipitation was performed with 10 μg sheared rat chromatin alongside 5
586 μg of *Schizosaccharomyces pombe* yeast chromatin, obtained as previously described (Mbogning
587 and Tanny, 2017). Chromatin was immunoprecipitated with an anti-FLAG M2 antibody (2 μg)

588 or equivalent amount of rabbit IgG alongside an anti-*Schizosaccharomyces pombe* H2B
589 antibody. RNAPII immunoprecipitation was performed with 20 μg of sheared rat chromatin
590 alongside 0.2 μg of *Schizosaccharomyces pombe* yeast chromatin. Chromatin was
591 immunoprecipitated with an anti-Rpb1 (8WG16) antibody. Localization was assessed by qPCR
592 with primers for specific genomic loci (**Supplemental Table 2**). All qPCR reactions were
593 performed using a Bio-Rad 1000 Series Thermal Cycling CFX96 Optical Reaction module and
594 iQ SYBR Green Supermix. Data analysis included subtracting the % Input of IgG control for
595 each treatment from the respective IP, followed by normalization to the % Input yeast *cdc2*$^{+}$ of
596 each FLAG IP or *act1*$^{+}$ for each RNAPII IP to account for differences in IP efficiencies.
597
598 **ChIP-seq immunoprecipitation and data analysis** - Immunoprecipitation in Cardiac
599 fibroblasts was performed as previously described, with minor modifications (Bolli et al., 2013).
600 Isolated nuclei were sonicated with a Diagenode BioRuptor™ UCD-200 (18 cycles, 30 s on/off,
601 high power) to shear chromatin. FLAG-Gβ_1 immunoprecipitation was performed with 40 μg of
602 sheared rat chromatin alongside 0.4 μg of chromatin from a *S. pombe* strain expressing FLAG-
603 Bdf2. RNAPII immunoprecipitation was performed using 20 μg sheared rat chromatin alongside
604 0.2 μg wild-type *S. pombe* chromatin. Chromatin was immunoprecipitated with an anti-FLAG
605 M2 antibody (2 μg) or anti-Rpb1 (8WG16) antibody (2 μg). Two biological replicates of FLAG-
606 Gβ_1 immunoprecipitation and three biological replicates of Rpb1 immunoprecipitation were
607 included. Following immunoprecipitation and DNA cleanup, libraries were prepared with the
608 NEBNext® Ultra™ II DNA Library Prep kit for Illumina and 50 bp single end reads obtained
609 with an Illumina HiSeq 4000 at the McGill University and Génome Québec Innovation Centre,
610 Montréal, Canada.

611 Reads were trimmed with TrimGalore (0.6.0) (Krueger, Martin, 2011) using the
612 following settings: --phred33 --length 36 -q 5 --stringency 1 -e 0.1. A Bowtie2 genome
613 comprised of the Ensembl rat reference genome (Rattus.norvegicus.Rnor.6.0.94) (Zerbino et al.,
614 2018) and *S. pombe* reference genome (Schizosaccharomyces_pombe.ASM294v2) was built
615 with the bowtie2-build function. Processed reads were aligned to the custom combined rat and *S.*
616 *pombe* genome with Bowtie2 (v2.3.5), followed by removal of low-quality mapped reads
617 (MAPQ < 10) and reads mapped to non-standard chromosomes with SAMtools (v1.9) (Li et al.,
618 2009). Duplicate reads were removed with Picard tools (v2.20.6, Broad Institute). Aligned reads
619 were separated into individual files for the rat or *S. pombe* genome respectively. For RNAPII
620 ChIP, peaks were called using macs2 (v2.1.1) with settings --broad and --broad-cutoff 0.1
621 (Zhang et al., 2008), reads extended by the fragment length determined by
622 phantompeakqualtools (v1.14) (Landt et al., 2012, Kharchenko et al., 2008), a scaling factor
623 estimated using the NCIS R package (Liang and Keles, 2012) and potential misassembled
624 regions of the rat genome blacklisted (Ramdas et al., 2019). RNAPII peaks were annotated with
625 HOMER (v4.11) (Heinz et al., 2010) and those protein-coding genes with RNAPII peaks in two
626 of three replicates in any treatment were used for subsequent analysis. BAM files of treatment
627 replicates were combined, input reads subtracted with the deepTools (Ramirez et al., 2014)
628 function bamCompare (--scaleFactorsMethod SES) and negative values set to 0. Lastly, values
629 were converted to counts per million mapped reads with library size adjusted by the total number
630 of reads aligned to the *S. pombe* genome. K-means clustering for genes with identified RNAPII
631 peaks and data visualization was performed with the deepTool's computeMatrix and plotProfile
632 functions. Gene ontology enrichment was performed using the R package topGO (v2.36.0).
633

634 **Statistical Analysis –** Statistical tests were performed using GraphPad Prism 8.0 software. For
635 quantifications of immunoprecipitation experiments, two-way analysis of variance (ANOVA)
636 followed by post-hoc Dunnett's test was used on quantifications of western blot bands, with all
637 multiple comparisons being made to vehicle-vehicle conditions. To analyse Ca^{2+} release
638 experiments, the dependent measure was the area under the curve (AUC), computed from
639 release-time data sets. AUC data were subjected to ANOVA and Dunnett's tests, using as a point
640 of comparison the siRNA control condition. For the FLAG-Gβ and RNAPII interaction in HEK
641 293F cells, one-sample t-tests were performed with a Bonferroni correction. Summary gene
642 expression of the fibrosis array qPCR was compared with a two-way ANOVA followed by post-
643 hoc t-tests with a Bonferroni correction. Individual gene expression from the fibrosis qPCR array
644 and Ctgf gene expression with in-house primers was assessed with a two-way ANOVA followed
645 by Bonferroni corrected post-hoc t-tests at individual time points. For validation of $G\beta_1$ and $G\beta_2$
646 knockdown in cardiac fibroblasts, fold changes over siRNA control were compared to siRNA
647 control using paired Student's t-tests. For FLAG-$G\beta_1$ ChIP-qPCR, independent paired Student t-
648 tests with a Bonferroni post-hoc correction were performed. A Fisher's exact test was used to
649 compare the proportion of cluster 1 genes in the list of genes with RNAPII peaks following Ang
650 II treatment in control or $G\beta_1$ knockdown conditions and to assess GO Term enrichment in
651 cluster 1 genes. Alpha was set at $p<0.05$ (2-tailed). All results are expressed as mean ± S.E.M,
652 and data are represented as pooled experiments whose sample sizes are indicated in figure
653 legends.
654
655
656

657 **FIGURE LEGENDS**

658 **Figure 1. Characterization of Gβγ-RNAPII in rat neonatal cardiac fibroblasts**. **(A)** Time
659 course of the Ang II-stimulated interaction between Gβγ and Rpb1. The ratio of Rpb1 co-
660 immunoprecipitated with $G\beta_{1-4}$ upon treatment of 1 μM Ang II treatment at the indicated
661 timepoints in cardiac fibroblasts was assessed. **(B)** Densitometry-based quantification of panel A
662 was used to determine the ratio of Rpb1 to $G\beta_{1-4}$ immunoprecipitated at each time point. The fold
663 change over the 0 min time point was then calculated. Data is representative of four independent
664 experiments. **(C)** Effect of AT1R antagonist losartan pre-treatment on the Ang II-mediated
665 interaction, demonstrating angiotensin receptor subtype selectivity. **(D)** Densitometry-based
666 quantification of AT1R antagonist effect on Ang II-induced interaction. The ratio of Rpb1
667 immunoprecipitated with $G\beta_{1-4}$ was determined for each condition and fold change over
668 DMSO/DMEM was calculated. Data is representative of three independent experiments. **(E)**
669 Assessment of the necessity of Gβγ import into the nucleus for interaction to occur upon AT1R
670 stimulation with Ang II. Cardiac fibroblasts were pretreated for 1 h with importazole prior to
671 Ang II stimulation. Data are representative of four independent experiments. **(F)** Densitometry-
672 based quantification of the Ang II induced interaction and the effect of nuclear import inhibition.
673 The ratio of Rpb1 to $G\beta_{1-4}$ immunoprecipitated was determined and normalized to fold change
674 over DMSO/DMEM treatment. In all panels, data represents mean ± S.E.M, * indicates $p<0.05$,
675 ** indicates $p<0.01$.

676

677 **Figure 2. Mechanistic analysis of Gβγ interactions with Rpb1 in rat neonatal cardiac**
678 **fibroblasts**. **(A-H)** Assessment of the effect of inhibition of signalling molecules and effectors
679 implicated in AT1R signalling on the induction of the Gβγ-RNAPII interaction in cardiac

680 fibroblasts. Concentrations of inhibitors and lengths of pre-treatment are indicated in each panel.
681 In all experiments, Ang II treatment was applied at a concentration of 1 μM for 75 min in order
682 to induce the interaction. Data shown is representative of between 3 and 6 independent co-
683 immunoprecipitation and western blot experiments. Corresponding quantification analyses of
684 inhibitor co-IP experiments are depicted in **Supplemental Figure 3**.
685
686 **Figure 3. Mechanistic analysis of carbachol-induced Gβγ interaction occurs in HEK 293**
687 **cells**. **(A-G)** HEK 293 cells were starved for 10-12 hours in DMEM without FBS and were then
688 pre-treated with the indicated inhibitors for the indicated times. Cells were subsequently treated
689 with 1 mM carbachol for 45 min, and the amount of Rpb1 co-immunoprecipitated with $G\beta_{1-4}$
690 was assessed by western blot. Data is representative of at least 3 independent experiments. The
691 associated quantifications of the co-IPs are represented in **Supplemental Figure 4**.
692
693 **Figure 4. Gβ subunit-specific effects on Ang II signalling and induction of Rpb1**
694 **interaction. (A)** Assessment of the effect of Gβ subunit knockdown by siRNA on the Gβγ-
695 RNAPII interaction upon AT1R stimulation. Cardiac fibroblasts were transfected with siRNA
696 control or siRNA to knockdown $G\beta_1$ or $G\beta_2$ and were then serum-deprived overnight before
697 treatment with Ang II for 75 min. Cells were assessed for Gβγ-RNAPII interaction by co-
698 immunoprecipitation and western blots. Data represents mean ± S.E.M. of 6-7 independent
699 experiments. **(B)** Densitometry-based quantification of knockdown experiments in (C) were
700 normalized as fold change over the respective siRNA-DMEM condition; data represents mean ±
701 S.E.M. of six independent experiments. **(C)** Traces of calcium release upon AT1R stimulation
702 with Ang II at the 10 s time point, with or without knockdown of either $G\beta_1$ or $G\beta_2$. Data

703 represents mean ± S.E.M. of fluorescence ratios of 340/516 emission readings to 360/516
704 emissions readings normalized to basal ratios of three independent experiments. **(D)** Area under
705 the curve analysis of the data obtained in panel A. * indicates $p<0.05$.
706
707 **Figure 5. Requirement of RNAPII transcription for Gβγ-RNAPII interaction in rat**
708 **neonatal cardiac fibroblasts**. Effect of Cdk7 inhibition with THZ1 **(A)** or Cdk9 inhibition with
709 iCdk9 **(B)** on Ang II-induced Gβγ-RNAPII interaction. Length of inhibitor pre-treatment is
710 indicated in each respective panel, and the extent of Gβγ-RNAPII interaction was assessed by
711 co-immunoprecipitation coupled to western blot analysis. Data is representative of three
712 independent experiments. Corresponding quantification analyses of inhibitor co-
713 immunoprecipitation experiments are depicted in **Supplemental Figure 7**. Cumulative $\log_2$(Fold
714 Change) of all genes detected by qPCR-based fibrosis array following treatment with 1 μM Ang
715 II lasting either 75 min **(C)** or 24 h **(D and E)**. Cardiac fibroblasts were transfected with 50 nM
716 of the indicated siRNA, and were serum-deprived for 12 h before Ang II treatment for the
717 indicated times. Cardiac fibroblasts were pre-treated for 30 min with 10 μM gallein prior to Ang
718 II. Ct values were normalized to the housekeeping genes Hprt1 and Ldha and the $\log_2$(fold
719 change) over control was determined. For each gene, the average $\log_2$(fold change) across three
720 independent experiments was plotted. *** indicates $p<0.001$, **** indicates $p<0.0001$.
721
722 **Figure 6**. **ChIP-seq for FLAG-Gβ1 and Rpb1 following 75 min Ang II treatment in cardiac**
723 **fibroblasts**. Cardiac fibroblasts were transduced with AAV1-FLAG-$G\beta_1$ or transfected with the
724 indicated siRNA followed by Ang II treatment (1 μM for 75 min). **(A)** Comparison of genes with
725 annotated RNAPII peaks following Ang II treatment and siRNA control or $G\beta_1$. FLAG-$G\beta_1$ **(B)**

726 or the Rpb1 subunit of RNAPII **(C)** were immunoprecipitated from crosslinked and sonicated
727 chromatin, followed by DNA purification and next-generation sequencing. Reads were
728 normalized to an exogenous *S. pombe* chromatin spike-in. Genes with a RNAPII peak annotated
729 by HOMER in two of the three replicates were used to identify two K-means clusters. **(D)** Top
730 four significant GO terms enriched in cluster 1. Individual FLAG-Gβ_1 or RNAPII tracks for two
731 genes from cluster 1, **(E)** Thbs1 or **(F)** Ctgf.
732
733 **Supplemental Figure 1. Induction of the Gβγ-RNAPII interaction in HEK 293 cells**. **(A)**
734 Time-course analysis of the induction of the Gβγ-RNAPII interaction. The amount of Rpb1 co-
735 immunoprecipitated with G$\beta_{1\text{-}4}$ from HEK 293 cells treated for the indicated times with 1 mM
736 carbachol was assessed by western blot for each time point. Data is representative of three
737 independent experiments. **(B)** Quantification of Gβγ-RNAPII time-course co-
738 immunoprecipitation. Densitometry-based analysis of bands corresponding to Rpb1 at each
739 timepoint was normalized to the band intensity of the amount of G$\beta_{1\text{-}4}$ immunoprecipitated to
740 yield ratios of Rpb1 pulled down with G$\beta_{1\text{-}4}$. **(C)** Assessing the Gβγ and Rpb1 interaction by
741 immunoprecipitation of Rpb1 with two different antibodies. Western blots are representative of
742 at least two independent experiments. Immunoprecipitation experiments demonstrating that
743 carbachol treatment does not induce interaction of Rpb1 with **(D)** G$\alpha_{q/11}$ nor **(E)** ERK1/2 in HEK
744 293 cells, and also does not alter the amount of G$\alpha_{q/11}$ or ERK1/2 interacting with Gβγ under
745 such conditions. **(F)** Assessment of interaction between G$\beta_{1\text{-}4}$ and Rpa194, the largest subunit of
746 RNA polymerase I. Data represents analysis of a time course experiment western blot performed
747 as in **Supplemental Figure 2A**. Data represents mean ± S.E.M; * indicates $p<0.05$, ** indicates
748 $p<0.01$.

749

750 **Supplemental Figure 2. Requirement for Gβγ nuclear transport for RNAPII interaction in**
751 **HEK 293 cells**. **(A)** Representative experiment assessing the requirement of importin-β
752 inhibition on the Gβγ-RNAPII interaction by sub-cellular fractionation and co-
753 immunoprecipitation. **(B)** Densitometry-based quantification of the carbachol induced interaction
754 and the effect of nuclear import inhibition on interaction induction. Data represents mean ±
755 S.E.M. of three independent experiments for black bars, and two independent experiments for
756 white bars (nuclear import inhibition conditions).

757

758 **Supplemental Figure 3. Quantitative analysis of the effects of inhibition of signalling**
759 **molecules downstream of AT1R activation**. **(A-H)** The relative quantities of Rpb1 co-
760 immunoprecipitated with $G\beta_{1-4}$ under different conditions depicted in **Figure 2** were quantified
761 using ImageJ and normalized to DMSO/DMEM control conditions. Data shown is representative
762 of (A) 3, (B) 6, (C) 3, (D) 4, (E) 5, (F) 5, (G) 4 or (H) 3 independent co-immunoprecipitation and
763 western blot experiments. Data is represented as fold change over respective controls and error
764 bars represent S.E.M. * indicates $p<0.05$, ** indicates $p<0.01$.

765

766 **Supplemental Figure 4. Quantitative analysis of the effects of inhibition of signalling**
767 **molecules downstream of M3-mAChR activation in HEK 293 cells**. **(A-G)** The relative
768 quantities of Rpb1 co-immunoprecipitated with $G\beta_{1-4}$ under different conditions depicted in
769 **Figure 3** were quantified using ImageJ and were normalized to amounts pulled down in
770 DMSO/DMEM control conditions. Data shown is representative of (A) 3, (B) 4, (C) 5, (D) 3, (E)
771 3, (F) 6 or (G) 4 independent co-immunoprecipitation and western blot experiments. Data is

772 represented as fold change over respective controls and error bars represent S.E.M. * indicates
773 $p<0.05$.
774
775 **Supplemental Figure 5. Assessment of specific Gβ subunits interacting with RNAPII upon**
776 **agonist stimulation in rat cardiac fibroblasts or in HEK 293 cells**. **(A)** Transcript levels for
777 GNB1, GNB2, GNB3, and GNB4 were assessed in cardiac fibroblasts by RT-qPCR. The Ct
778 values for each gene transcript were normalized to the house keeping U6 snRNA gene transcript
779 for comparison. Data represents mean ± S.E.M for 3-4 independent experiments. **(B)** $G\beta_1$ and
780 $G\beta_2$ were immunoprecipitated with isoform specific antibodies from cardiac fibroblasts lysates
781 treated with 1 μM Ang II for 75 min. The amount of Rpb1 pulled down with either Gβ isoform
782 was assessed by western blot. **(C)** Assessment of specific FLAG-tagged Gβ isoforms interaction
783 with Rpb1 under conditions of M3-mAChR stimulation with carbachol in HEK 293 cells. The
784 amount of Rpb1 interacting with each Gβ isoform was assessed by western blot following FLAG
785 immunoprecipitation. **(D)** Densitometry-based quantification of the ratio of Rpb1 co-
786 immunoprecipitated with the indicated FLAG-tagged Gβ subunit. The ratio of Rpb1 to FLAG-
787 $G\beta_x$ immunoprecipitated was determined and normalized to fold change over DMEM treatment.
788 Data represents mean ± S.E.M for four independent replicates; * indicates $p<0.01$
789
790 **Supplemental Figure 6. Validation of RNAi knockdown of $G\beta_1$ and $G\beta_2$.** Validation of $G\beta_1$
791 and $G\beta_2$ mRNA **(A)** and protein **(B)** knockdown with siRNA in rat neonatal cardiac fibroblasts.
792 Rat neonatal cardiac fibroblasts were transfected with 50 nM siRNA control, $G\beta_1$ or $G\beta_2$ for 72
793 hours, serum-deprived for 12 h and RNA or protein collected as described in *Methods*. Data in
794 (A) represents mean ± S.E.M for four independent experiments; * Ct values were normalized to

795 the housekeeping U6 snRNA transcript and fold change over siRNA control determined using
796 the $2^{-\Delta\Delta Ct}$. ** indicates p<0.001 and **** indicates p<0.0001.
797
798 **Supplemental Figure 7. Quantitative analysis of the effect of transcriptional regulator**
799 **inhibition on the Gβγ-RNAPII interaction in cardiac fibroblasts. (A-B)** The relative
800 quantities of Rpb1 co-immunoprecipitated with $G\beta_{1-4}$ under conditions depicted in Figure 5A
801 (THZ1) and B (iCdk9) were quantified and normalized to DMSO/DMEM control conditions.
802 Data shown is representative of between three to six independent co-immunoprecipitation and
803 western blot experiments. Data represents mean ± S.E.M. * indicates p<0.05.
804
805 **Supplemental Figure 8. Validation of heterologously expressed FLAG-tagged $G\beta_1$ in rat**
806 **neonatal cardiac fibroblasts. (A)** Assessment of Rpb1 co-immunoprecipitated with FLAG-$G\beta_1$
807 following 75 min treatment of 1 μM Ang II in rat neonatal cardiac fibroblasts. Cardiac
808 fibroblasts were transduced with AAV1-FLAG-$G\beta_1$ prior to treatment with 1 μM Ang II. **(B)**
809 Densitometry-based quantification of the ratio of Rpb1 co-immunoprecipitated with FLAG-$G\beta_1$.
810 The ratio of Rpb1 to FLAG-$G\beta_1$ was calculated and normalized as fold change over DMEM
811 condition. Data is represented as mean ± S.E.M for four independent experiments. Assessing
812 changes in FLAG-$G\beta_1$ **(C)** or **(D)** Rpb1 occupancy along Ctgf following 75 min treatment with 1
813 μM Ang II. FLAG-$G\beta_1$ or Rpb1 was immunoprecipitated from crosslinked and sonicated
814 chromatin, DNA purified and quantified by qPCR. Data is represented as mean ± S.E.M for 4-6
815 independent experiments, * indicates p<0.05. **(E)** Validation of Ctgf gene expression with
816 primers distinct from those used in the Qiagen RT^2 Profiler™ PCR array. Data represents mean
817 ± S.E.M for four independent experiments, * indicates p<0.05.

818

819

820 **Supplemental Figure 9. Schema summarizing signalling events regulating the agonist**
821 **induced Gβγ interaction with RNAPII.** Signalling cascade downstream of AT1R in cardiac
822 fibroblasts or M3 muscarinic receptors in HEK 293F cells regulating the interaction. Signalling
823 pathways were determined by assessing Gβγ-RNAPII interactions by co-immunoprecipitation
824 and western blot as shown in **Figure 2** and **Supplemental Figure 3** for cardiac fibroblasts and
825 **Figure 3** and **Supplemental Figure 4** for HEK 293F cells.

826

827

828

829

830

831

832

833

834

835

836

837

838

839

840

841 **Tables**

842 **Supplemental Table 1. Summary of fibrosis RT-qPCR array results**. This table summarizes
843 gene expression changes measured using the Qiagen RT^2 Profiler^{TM} PCR Array at 75 min and 24
844 h Ang II stimulation. Genes were considered to have altered expression with fold changes ≥ 1.5
845 or ≤ 0.5 compared to DMEM/siRNA control conditions at the respective time point. In
846 parenthesis are the number of genes with a significant ($p<0.05$) change in expression compared
847 to DMEM/siRNA control at the respective time point. Two-way ANOVA followed by post-hoc
848 t-test comparisons with Bonferroni correction was performed for each gene individually. Data is
849 representative of three independent biological replicates.

Time	siRNA	Treatment	Upregulated	Downregulated
75 min	Control	DMEM	0	0
		1 μM Ang II	7(5)	0
	Gnb1	DMEM	4(1)	1
		1 μM Ang II	10(6)	2
24 h	Control	DMEM	0	0
		1 μM Ang II	37(7)	0
	Gnb1	DMEM	26(2)	1
		1 μM Ang II	53(13)	0
	Gnb2	DMEM	7	1
		1 μM Ang II	44(11)	0

850
851
852
853
854
855
856
857

858 **Supplemental Table 2. List of primers used to assess gene expression by RT-qPCR and**
859 **ChIP-qPCR in cardiac fibroblasts**. Forward and reverse primers were used at a concentration
860 of 300 nM for each qPCR reaction. Primer sequences were designed using NCBI's Primer-
861 BLAST tool and validated by analysis of standard curve qPCR assays performed in-house.

Target	Forward (5' -> 3')	Reverse (5' -> 3')
U6 snRNA	TGGAACGATACAGAGAAGATTAG	GAATTTGCGTGTCATCCTTG
$G\beta_1$	CTCATGACCTACTCCCATGA	TCAGCTTTGAGTGCATCC
$G\beta_2$	CAGCTACACCACTAACAAGG	CTCTCGGGTCTTGAGACTAT
$G\beta_3$	CTCCTTAGGGTCAGTCTTCTAT	AAAGGCACACTCCCATAATC
$G\beta_4$	GGTGGTCAAAGAAACAATCAAG	GTCTGTCGGGATAGGGATAA
Ctgf	TGCATCCTCCTACCGCGTCC	GAGGCTGATGGGACCTGCGA
Ctgf TSS	CAGACCCACTCCAGCTCCGA	GTGGCTCCTGGGGTTGTCCA
Ctgf Exon	TCAAGCTGCCCGGGAAATGC	GCGGTCCTTGGGCTCATCAC
Ctgf 3' End	AATGGCTTGCTCAGGGTAACTGG	AACTGCCTCCCAAACCAGTCATAG
$cdc2^+$	ATCATTCTCGCATCTCTATTA	ATTCTCCATTGCAAACCACTA
$act1^+$	GGTTGCTCAATGTTATCCGTTTC	TGATAAAGCCACACACAGCGTTA

862

863 **Acknowledgements**

864 This work was supported by a grant from the Heart and Stroke Foundation of Canada (G-
865 15-0008938) to T.E.H and J.C.T, a grant from Canadian Institute of Health Science (CIHR)
866 (MOP 130362) to J.C.T. and a grant from CIHR (PJT-159687) to T.E.H. R.M. and S.M.K were
867 supported by studentships from the McGill-CIHR Drug Development Training Program and the
868 McGill Faculty of Medicine. We thank Dr. Ron Taussig (UT Southwestern), Dr. Nathanael S.
869 Gray, and Novartis for providing materials instrumental to this study. Lastly, we thank all the
870 members of the Hébert and Tanny labs for discussion and critical reading of the manuscript.

871

872

873

874

875 **Author Contributions**

876 S.M.K, R.D.M, J.C.T, and T.E.H designed the experiments and wrote the manuscript. S.M.K,
877 R.D.M, S.G, C.B, J.J.T, A.Z, S.M, and P.T conducted experiments. S.M.K, R.DM and C.B
878 analyzed experiments. R.D.M, J.J.T, J.C.T and T.E.H edited the manuscript.

879

880 **Declaration of Interests**

881 None

882

883 **References**

884 AHMED, M. S., ØIE, E., VINGE, L. E., YNDESTAD, A., ØYSTEIN ANDERSEN, G., ANDERSSON, Y.,
885 ATTRAMADAL, T. & ATTRAMADAL, H. 2004. Connective tissue growth factor—a novel
886 mediator of angiotensin II-stimulated cardiac fibroblast activation in heart failure in rats.
887 *Journal of Molecular and Cellular Cardiology,* 36**,** 393-404.
888 ANAND, P., BROWN, J. D., LIN, C. Y., QI, J., ZHANG, R., ARTERO, P. C., ALAITI, M. A., BULLARD, J.,
889 ALAZEM, K., MARGULIES, K. B., CAPPOLA, T. P., LEMIEUX, M., PLUTZKY, J., BRADNER, J. E.
890 & HALDAR, S. M. 2013. BET bromodomains mediate transcriptional pause release in
891 heart failure. *Cell,* 154**,** 569-82.
892 BHATNAGAR, A., UNAL, H., JAGANNATHAN, R., KAVETI, S., DUAN, Z. H., YONG, S., VASANJI, A.,
893 KINTER, M., DESNOYER, R. & KARNIK, S. S. 2013. Interaction of G-protein βγ complex
894 with chromatin modulates GPCR-dependent gene regulation. *PLoS One,* 8**,** e52689.
895 BOLLI, P., VARDABASSO, C., BERNSTEIN, E. & CHAUDHRY, H. W. 2013. Chromatin
896 immunoprecipitation of adult murine cardiomyocytes. *Curr Protoc Cell Biol,* Chapter 17**,**
897 Unit17 14.
898 BURGER, C. & NASH, K. R. 2016. Small-Scale Recombinant Adeno-Associated Virus Purification.
899 *Methods Mol Biol,* 1382**,** 95-106.
900 CALDERONE, A., THAIK, C. M., TAKAHASHI, N., CHANG, D. L. & COLUCCI, W. S. 1998. Nitric oxide,
901 atrial natriuretic peptide, and cyclic GMP inhibit the growth-promoting effects of
902 norepinephrine in cardiac myocytes and fibroblasts. *J Clin Invest,* 101**,** 812-8.
903 CAMPBELL, S. E. & KATWA, L. C. 1997. Angiotensin II stimulated expression of transforming
904 growth factor-β1 in cardiac fibroblasts and myofibroblasts. *J Mol Cell Cardiol,* 29**,** 1947-
905 58.
906 CAMPDEN, R., AUDET, N. & HÉBERT, T. E. 2015a. Nuclear G Protein Signaling: New Tricks for Old
907 Dogs. *Journal of Cardiovascular Pharmacology,* 65**,** 110-122.
908 CAMPDEN, R., PÉTRIN, D., ROBITAILLE, M., AUDET, N., GORA, S., ANGERS, S. & HÉBERT, T.
909 2015b. Tandem Affinity Purification to Identify Cytosolic and Nuclear Gβγ-Interacting
910 Proteins. *In:* ALLEN, B. G. & HÉBERT, T. E. (eds.) *Nuclear G-Protein Coupled Receptors.*
911 Springer New York.
912 CHENG, T.-H., CHENG, P.-Y., SHIH, N.-L., CHEN, I.-B., WANG, D. L. & CHEN, J.-J. 2003.
913 Involvement of reactive oxygen species in angiotensin II-induced endothelin-1 gene
914 expression in rat cardiac fibroblasts. *Journal of the American College of Cardiology,* 42**,**
915 1845-1854.
916 CHINTALGATTU, V. & KATWA, L. C. 2009. Role of protein kinase C-δ in angiotensin II induced
917 cardiac fibrosis. *Biochemical and Biophysical Research Communications,* 386**,** 612-616.
918 DANG, M. Q., ZHAO, X. C., LAI, S., WANG, X., WANG, L., ZHANG, Y. L., LIU, Y., YU, X. H., LIU, Y., LI,
919 H. H. & XIA, Y. L. 2015. Gene expression profile in the early stage of angiotensin II-
920 induced cardiac remodeling: a time series microarray study in a mouse model. *Cell*
921 *Physiol Biochem,* 35**,** 467-76.
922 DEVOST, D., SLENO, R., PETRIN, D., ZHANG, A., SHINJO, Y., OKDE, R., AOKI, J., INOUE, A. &
923 HÉBERT, T. E. 2017. Conformational Profiling of the AT1 Angiotensin II Receptor Reflects
924 Biased Agonism, G Protein Coupling, and Cellular Context. *J Biol Chem,* 292**,** 5443-5456.

925 DOBACZEWSKI, M., BUJAK, M., LI, N., GONZALEZ-QUESADA, C., MENDOZA, L. H., WANG, X. F. &
926 FRANGOGIANNIS, N. G. 2010. Smad3 signaling critically regulates fibroblast phenotype
927 and function in healing myocardial infarction. *Circ Res,* 107**,** 418-28.
928 DUAN, Q., MCMAHON, S., ANAND, P., SHAH, H., THOMAS, S., SALUNGA, H. T., HUANG, Y.,
929 ZHANG, R., SAHADEVAN, A., LEMIEUX, M. E., BROWN, J. D., SRIVASTAVA, D., BRADNER,
930 J. E., MCKINSEY, T. A. & HALDAR, S. M. 2017. BET bromodomain inhibition suppresses
931 innate inflammatory and profibrotic transcriptional networks in heart failure. *Sci Transl*
932 *Med,* 9.
933 DUPRÉ DJ, R. M., REBOIS RV, HÉBERT TE 2009. The role of Gβγ subunits in the organization,
934 assembly and function of GPCR signaling complexes. *Annu. Rev. Pharmacol. Toxicol.,* 49**,**
935 31-56.
936 FU, X., KHALIL, H., KANISICAK, O., BOYER, J. G., VAGNOZZI, R. J., MALIKEN, B. D., SARGENT, M.
937 A., PRASAD, V., VALIENTE-ALANDI, I., BLAXALL, B. C. & MOLKENTIN, J. D. 2018.
938 Specialized fibroblast differentiated states underlie scar formation in the infarcted
939 mouse heart. *J Clin Invest,* 128**,** 2127-2143.
940 GAO, X., HE, X., LUO, B., PENG, L., LIN, J. & ZUO, Z. 2009. Angiotensin II increases collagen I
941 expression via transforming growth factor-β1 and extracellular signal-regulated kinase in
942 cardiac fibroblasts. *European Journal of Pharmacology,* 606**,** 115-120.
943 GREENWOOD, I. A. & STOTT, J. B. 2019. The Gβ1 and Gβ3 Subunits Differentially Regulate Rat
944 Vascular Kv7 Channels. *Front Physiol,* 10**,** 1573.
945 HEINZ, S., BENNER, C., SPANN, N., BERTOLINO, E., LIN, Y. C., LASLO, P., CHENG, J. X., MURRE, C.,
946 SINGH, H. & GLASS, C. K. 2010. Simple combinations of lineage-determining
947 transcription factors prime cis-regulatory elements required for macrophage and B cell
948 identities. *Mol Cell,* 38**,** 576-89.
949 KAMAL, F. A., SMRCKA, A. V. & BLAXALL, B. C. 2011. Taking the heart failure battle inside the
950 cell: small molecule targeting of Gβγ subunits. *J Mol Cell Cardiol,* 51**,** 462-7.
951 KAMAL, F. A., TRAVERS, J. G., SCHAFER, A. E., MA, Q., DEVARAJAN, P. & BLAXALL, B. C. 2017. G
952 Protein-Coupled Receptor-G-Protein βγ-Subunit Signaling Mediates Renal Dysfunction
953 and Fibrosis in Heart Failure. *J Am Soc Nephrol,* 28**,** 197-208.
954 KAWANO, H., DO, Y. S., KAWANO, Y., STARNES, V., BARR, M., LAW, R. E. & HSUEH, W. A. 2000.
955 Angiotensin II has multiple profibrotic effects in human cardiac fibroblasts. *Circulation,*
956 101**,** 1130-7.
957 KHAN, S. M., MIN, A., GORA, S., HOURANIEH, G. M., CAMPDEN, R., ROBITAILLE, M., TRIEU, P.,
958 PÉTRIN, D., JACOBI, A. M., BEHLKE, M. A., ANGERS, S. & HÉBERT, T. E. 2015. Gβ4γ1 as a
959 modulator of M3 muscarinic receptor signalling and novel roles of Gβ1 subunits in the
960 modulation of cellular signalling. *Cellular Signalling,* 27**,** 1597-1608.
961 KHAN, S. M., SLENO, R., GORA, S., ZYLBERGOLD, P., LAVERDURE, J.-P., LABBÉ, J.-C., MILLER, G. J.
962 & HÉBERT, T. E. 2013. The Expanding Roles of Gβγ Subunits in G Protein–Coupled
963 Receptor Signaling and Drug Action. *Pharmacological Reviews,* 65**,** 545-577.
964 KHARCHENKO, P. V., TOLSTORUKOV, M. Y. & PARK, P. J. 2008. Design and analysis of ChIP-seq
965 experiments for DNA-binding proteins. *Nat Biotechnol,* 26**,** 1351-9.
966 KRUEGER, F. *Trim Galore!* [Online]. Available:
967 http://www.bioinformatics.babraham.ac.uk/projects/trim_galore/ [Accessed].

968 KWIATKOWSKI, N., ZHANG, T., RAHL, P. B., ABRAHAM, B. J., REDDY, J., FICARRO, S. B., DASTUR,
969 A., AMZALLAG, A., RAMASWAMY, S., TESAR, B., JENKINS, C. E., HANNETT, N. M.,
970 MCMILLIN, D., SANDA, T., SIM, T., KIM, N. D., LOOK, T., MITSIADES, C. S., WENG, A. P.,
971 BROWN, J. R., BENES, C. H., MARTO, J. A., YOUNG, R. A. & GRAY, N. S. 2014. Targeting
972 transcription regulation in cancer with a covalent CDK7 inhibitor. *Nature,* 511**,** 616-20.
973 LANDT, S. G., MARINOV, G. K., KUNDAJE, A., KHERADPOUR, P., PAULI, F., BATZOGLOU, S.,
974 BERNSTEIN, B. E., BICKEL, P., BROWN, J. B., CAYTING, P., CHEN, Y., DESALVO, G.,
975 EPSTEIN, C., FISHER-AYLOR, K. I., EUSKIRCHEN, G., GERSTEIN, M., GERTZ, J., HARTEMINK,
976 A. J., HOFFMAN, M. M., IYER, V. R., JUNG, Y. L., KARMAKAR, S., KELLIS, M.,
977 KHARCHENKO, P. V., LI, Q., LIU, T., LIU, X. S., MA, L., MILOSAVLJEVIC, A., MYERS, R. M.,
978 PARK, P. J., PAZIN, M. J., PERRY, M. D., RAHA, D., REDDY, T. E., ROZOWSKY, J., SHORESH,
979 N., SIDOW, A., SLATTERY, M., STAMATOYANNOPOULOS, J. A., TOLSTORUKOV, M. Y.,
980 WHITE, K. P., XI, S., FARNHAM, P. J., LIEB, J. D., WOLD, B. J. & SNYDER, M. 2012. ChIP-seq
981 guidelines and practices of the ENCODE and modENCODE consortia. *Genome Res,* 22**,**
982 1813-31.
983 LEE, A. A., DILLMANN, W. H., MCCULLOCH, A. D. & VILLARREAL, F. J. 1995. Angiotensin II
984 stimulates the autocrine production of transforming growth factor-β 1 in adult rat
985 cardiac fibroblasts. *J Mol Cell Cardiol,* 27**,** 2347-57.
986 LEHMANN, D. M., SENEVIRATNE, A. M. & SMRCKA, A. V. 2008. Small molecule disruption of G
987 protein βγ subunit signaling inhibits neutrophil chemotaxis and inflammation. *Mol*
988 *Pharmacol,* 73**,** 410-8.
989 LI, H., HANDSAKER, B., WYSOKER, A., FENNELL, T., RUAN, J., HOMER, N., MARTH, G., ABECASIS,
990 G., DURBIN, R. & GENOME PROJECT DATA PROCESSING, S. 2009. The Sequence
991 Alignment/Map format and SAMtools. *Bioinformatics,* 25**,** 2078-9.
992 LIANG, K. & KELES, S. 2012. Normalization of ChIP-seq data with control. *BMC Bioinformatics,*
993 13**,** 199.
994 LIN, Y. & SMRCKA, A. V. 2011. Understanding molecular recognition by G protein βγ subunits on
995 the path to pharmacological targeting. *Mol Pharmacol,* 80**,** 551-7.
996 LIU, X., KRAUS, W. L. & BAI, X. 2015. Ready, pause, go: regulation of RNA polymerase II pausing
997 and release by cellular signaling pathways. *Trends Biochem Sci,* 40**,** 516-25.
998 LU, H., XUE, Y., YU, G. K., ARIAS, C., LIN, J., FONG, S., FAURE, M., WEISBURD, B., JI, X., MERCIER,
999 A., SUTTON, J., LUO, K., GAO, Z. & ZHOU, Q. 2015. Compensatory induction of MYC
1000 expression by sustained CDK9 inhibition via a BRD4-dependent mechanism. *Elife,* 4**,**
1001 e06535.
1002 MA, Z. G., YUAN, Y. P., WU, H. M., ZHANG, X. & TANG, Q. Z. 2018. Cardiac fibrosis: new insights
1003 into the pathogenesis. *Int J Biol Sci,* 14**,** 1645-1657.
1004 MARTIN, M. 2011. Cutadapt removes adapter sequences from high-throughput sequencing
1005 reads. *2011,* 17**,** 3.
1006 MBOGNING, J. & TANNY, J. C. 2017. Chromatin Immunoprecipitation of Histone Modifications
1007 in Fission Yeast. *Methods Mol Biol,* 1528**,** 199-210.
1008 MURPHY, A. M., WONG, A. L. & BEZUHLY, M. 2015. Modulation of angiotensin II signaling in the
1009 prevention of fibrosis. *Fibrogenesis Tissue Repair,* 8**,** 7.
1010 NAMKUNG, Y., LEGOUILL, C., KUMAR, S., CAO, Y., TEIXEIRA, L. B., LUKASHEVA, V., GIUBILARO, J.,
1011 SIMOES, S. C., LONGPRE, J. M., DEVOST, D., HÉBERT, T. E., PINEYRO, G., LEDUC, R.,

1012 COSTA-NETO, C. M., BOUVIER, M. & LAPORTE, S. A. 2018. Functional selectivity profiling
1013 of the angiotensin II type 1 receptor using pathway-wide BRET signaling sensors. *Sci*
1014 *Signal,* 11.
1015 OLSON, E. R., SHAMHART, P. E., NAUGLE, J. E. & MESZAROS, J. G. 2008. Angiotensin II-Induced
1016 Extracellular Signal-Regulated Kinase 1/2 Activation Is Mediated by Protein Kinase Cδ
1017 and Intracellular Calcium in Adult Rat Cardiac Fibroblasts. *Hypertension,* 51**,** 704-711.
1018 PARK, D., JHON, D. Y., LEE, C. W., LEE, K. H. & RHEE, S. G. 1993. Activation of phospholipase C
1019 isozymes by G protein βγ subunits. *J Biol Chem,* 268**,** 4573-6.
1020 PARK, J. G., MUISE, A., HE, G. P., KIM, S. W. & RO, H. S. 1999. Transcriptional regulation by the
1021 γ5 subunit of a heterotrimeric G protein during adipogenesis. *Embo J,* 18**,** 4004-12.
1022 PASSIER, R. C., SMITS, J. F., VERLUYTEN, M. J. & DAEMEN, M. J. 1996. Expression and
1023 localization of renin and angiotensinogen in rat heart after myocardial infarction. *Am J*
1024 *Physiol,* 271**,** H1040-8.
1025 RAMDAS, S., OZEL, A. B., TREUTELAAR, M. K., HOLL, K., MANDEL, M., WOODS, L. C. S. & LI, J. Z.
1026 2019. Extended regions of suspected mis-assembly in the rat reference genome. *Sci*
1027 *Data,* 6**,** 39.
1028 RAMIREZ, F., DUNDAR, F., DIEHL, S., GRUNING, B. A. & MANKE, T. 2014. deepTools: a flexible
1029 platform for exploring deep-sequencing data. *Nucleic Acids Res,* 42**,** W187-91.
1030 ROBITAILLE, M., GORA, S., WANG, Y., GOUPIL, E., PETRIN, D., DEL DUCA, D., VILLENEUVE, L. R.,
1031 ALLEN, B. G., LAPORTE, S. A., BERNARD, D. J. & HÉBERT, T. E. 2010. Gβγ is a negative
1032 regulator of AP-1 mediated transcription. *Cell Signal,* 22**,** 1254-66.
1033 ROSENKRANZ, S. 2004. TGF-β1 and angiotensin networking in cardiac remodeling. *Cardiovasc*
1034 *Res,* 63**,** 423-32.
1035 SANO, M., ABDELLATIF, M., OH, H., XIE, M., BAGELLA, L., GIORDANO, A., MICHAEL, L. H.,
1036 DEMAYO, F. J. & SCHNEIDER, M. D. 2002. Activation and function of cyclin T-Cdk9
1037 (positive transcription elongation factor-b) in cardiac muscle-cell hypertrophy. *Nat Med,*
1038 8**,** 1310-7.
1039 SAULIERE, A., BELLOT, M., PARIS, H., DENIS, C., FINANA, F., HANSEN, J. T., ALTIE, M. F.,
1040 SEGUELAS, M. H., PATHAK, A., HANSEN, J. L., SENARD, J. M. & GALES, C. 2012.
1041 Deciphering biased-agonism complexity reveals a new active AT1 receptor entity. *Nat*
1042 *Chem Biol,* 8**,** 622-30.
1043 SAYED, D., HE, M., YANG, Z., LIN, L. & ABDELLATIF, M. 2013. Transcriptional regulation patterns
1044 revealed by high resolution chromatin immunoprecipitation during cardiac hypertrophy.
1045 *J Biol Chem,* 288**,** 2546-58.
1046 SCHRAGE, R., SCHMITZ, A. L., GAFFAL, E., ANNALA, S., KEHRAUS, S., WENZEL, D., BULLESBACH,
1047 K. M., BALD, T., INOUE, A., SHINJO, Y., GALANDRIN, S., SHRIDHAR, N., HESSE, M.,
1048 GRUNDMANN, M., MERTEN, N., CHARPENTIER, T. H., MARTZ, M., BUTCHER, A. J.,
1049 SLODCZYK, T., ARMANDO, S., EFFERN, M., NAMKUNG, Y., JENKINS, L., HORN, V.,
1050 STOSSEL, A., DARGATZ, H., TIETZE, D., IMHOF, D., GALES, C., DREWKE, C., MULLER, C. E.,
1051 HOLZEL, M., MILLIGAN, G., TOBIN, A. B., GOMEZA, J., DOHLMAN, H. G., SONDEK, J.,
1052 HARDEN, T. K., BOUVIER, M., LAPORTE, S. A., AOKI, J., FLEISCHMANN, B. K., MOHR, K.,
1053 KONIG, G. M., TUTING, T. & KOSTENIS, E. 2015. The experimental power of FR900359 to
1054 study Gq-regulated biological processes. *Nat Commun,* 6**,** 10156.

1055 SHU, J., LIU, Z., JIN, L. & WANG, H. 2018. An RNAsequencing study identifies candidate genes for
1056 angiotensin IIinduced cardiac remodeling. *Mol Med Rep,* 17**,** 1954-1962.
1057 SMRCKA, A. V. 2008. G protein βγ subunits: central mediators of G protein-coupled receptor
1058 signaling. *Cell Mol Life Sci,* 65.
1059 SMRCKA, A. V., LEHMANN, D. M. & DESSAL, A. L. 2008. G protein βγ subunits as targets for
1060 small molecule therapeutic development. *Comb Chem High Throughput Screen,* 11**,** 382-
1061 95.
1062 SPIEGELBERG, B. D. & HAMM, H. E. 2005. Gβγ binds histone deacetylase 5 (HDAC5) and inhibits
1063 its transcriptional co-repression activity. *J Biol Chem,* 280**,** 41769-76.
1064 STRATTON, M. S., LIN, C. Y., ANAND, P., TATMAN, P. D., FERGUSON, B. S., WICKERS, S. T.,
1065 AMBARDEKAR, A. V., SUCHAROV, C. C., BRADNER, J. E., HALDAR, S. M. & MCKINSEY, T.
1066 A. 2016. Signal-Dependent Recruitment of BRD4 to Cardiomyocyte Super-Enhancers Is
1067 Suppressed by a MicroRNA. *Cell Rep,* 16**,** 1366-1378.
1068 SUN, Y. & WEBER, K. T. 1996. Angiotensin converting enzyme and myofibroblasts during tissue
1069 repair in the rat heart. *J Mol Cell Cardiol,* 28**,** 851-8.
1070 TRAVERS, J. G., KAMAL, F. A., ROBBINS, J., YUTZEY, K. E. & BLAXALL, B. C. 2016. Cardiac Fibrosis:
1071 The Fibroblast Awakens. *Circ Res,* 118**,** 1021-40.
1072 TRAVERS, J. G., KAMAL, F. A., VALIENTE-ALANDI, I., NIEMAN, M. L., SARGENT, M. A., LORENZ, J.
1073 N., MOLKENTIN, J. D. & BLAXALL, B. C. 2017. Pharmacological and Activated Fibroblast
1074 Targeting of Gβγ-GRK2 After Myocardial Ischemia Attenuates Heart Failure Progression.
1075 *J Am Coll Cardiol,* 70**,** 958-971.
1076 WEBER, K. T. & DIEZ, J. 2016. Targeting the Cardiac Myofibroblast Secretome to Treat
1077 Myocardial Fibrosis in Heart Failure. *Circ Heart Fail,* 9.
1078 WEBER, K. T., SUN, Y., BHATTACHARYA, S. K., AHOKAS, R. A. & GERLING, I. C. 2013.
1079 Myofibroblast-mediated mechanisms of pathological remodelling of the heart. *Nat Rev*
1080 *Cardiol,* 10**,** 15-26.
1081 YANG, J., TIAN, B. & BRASIER, A. R. 2017. Targeting Chromatin Remodeling in Inflammation and
1082 Fibrosis. *Adv Protein Chem Struct Biol,* 107**,** 1-36.
1083 YIM, Y. Y., BETKE, K. M., MCDONALD, W. H., GILSBACH, R., CHEN, Y., HYDE, K., WANG, Q., HEIN,
1084 L. & HAMM, H. 2019. The in vivo specificity of synaptic Gβ and Gγ subunits to the
1085 alpha2a adrenergic receptor at CNS synapses. *Sci Rep,* 9**,** 1718.
1086 ZERBINO, D. R., ACHUTHAN, P., AKANNI, W., AMODE, M. R., BARRELL, D., BHAI, J., BILLIS, K.,
1087 CUMMINS, C., GALL, A., GIRON, C. G., GIL, L., GORDON, L., HAGGERTY, L., HASKELL, E.,
1088 HOURLIER, T., IZUOGU, O. G., JANACEK, S. H., JUETTEMANN, T., TO, J. K., LAIRD, M. R.,
1089 LAVIDAS, I., LIU, Z., LOVELAND, J. E., MAUREL, T., MCLAREN, W., MOORE, B., MUDGE, J.,
1090 MURPHY, D. N., NEWMAN, V., NUHN, M., OGEH, D., ONG, C. K., PARKER, A., PATRICIO,
1091 M., RIAT, H. S., SCHUILENBURG, H., SHEPPARD, D., SPARROW, H., TAYLOR, K.,
1092 THORMANN, A., VULLO, A., WALTS, B., ZADISSA, A., FRANKISH, A., HUNT, S. E.,
1093 KOSTADIMA, M., LANGRIDGE, N., MARTIN, F. J., MUFFATO, M., PERRY, E., RUFFIER, M.,
1094 STAINES, D. M., TREVANION, S. J., AKEN, B. L., CUNNINGHAM, F., YATES, A. & FLICEK, P.
1095 2018. Ensembl 2018. *Nucleic Acids Res,* 46**,** D754-D761.
1096 ZHANG, J. H., BARR, V. A., MO, Y., ROJKOVA, A. M., LIU, S. & SIMONDS, W. F. 2001. Nuclear
1097 localization of G protein β 5 and regulator of G protein signaling 7 in neurons and brain.
1098 *J Biol Chem,* 276**,** 10284-9.

1099 ZHANG, Y., LIU, T., MEYER, C. A., EECKHOUTE, J., JOHNSON, D. S., BERNSTEIN, B. E., NUSBAUM,
1100 C., MYERS, R. M., BROWN, M., LI, W. & LIU, X. S. 2008. Model-based analysis of ChIP-Seq
1101 (MACS). *Genome Biol,* 9**,** R137.
1102 ZHOU, Q., LI, T. & PRICE, D. H. 2012. RNA polymerase II elongation control. *Annu Rev Biochem,*
1103 81**,** 119-43.
1104

Figure 1.

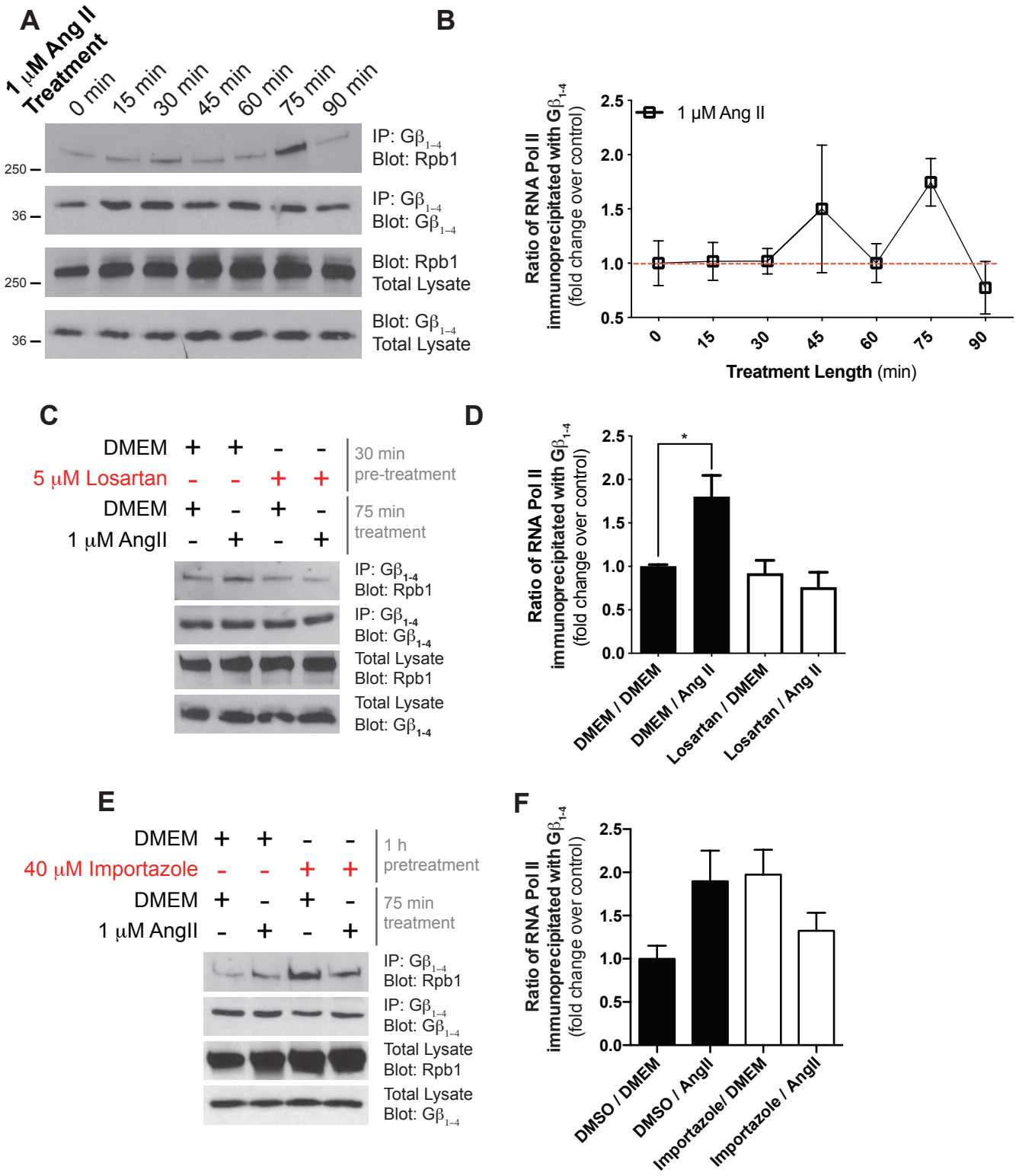
A
1 μM Ang II Treatment
0 min
15 min
30 min
45 min
60 min
75 min
90 min
250
36
250
36
IP: Gβ1–4
Blot: Rpb1
IP: Gβ1–4
Blot: Gβ1–4
Blot: Rpb1
Total Lysate
Blot: Gβ1–4
Total Lysate
B
1 μM Ang II
Ratio of RNA Pol II immunoprecipitated with Gβ1-4 (fold change over control)
2.5
2.0
1.5
1.0
0.5
0
15
30
45
60
75
90
Treatment Length (min)
C
DMEM + + - -
5 μM Losartan - - + +
30 min pre-treatment
DMEM + - + -
1 μM AngII - + - +
75 min treatment
IP: Gβ1-4
Blot: Rpb1
IP: Gβ1-4
Blot: Gβ1-4
Total Lysate
Blot: Rpb1
Total Lysate
Blot: Gβ1-4
D
Ratio of RNA Pol II immunoprecipitated with Gβ1-4 (fold change over control)
*
2.5
2.0
1.5
1.0
0.5
0.0
DMEM / DMEM
DMEM / Ang II
Losartan / DMEM
Losartan / Ang II
E
DMEM + + - -
40 μM Importazole - - + +
1 h pretreatment
DMEM + - + -
1 μM AngII - + - +
75 min treatment
IP: Gβ1–4
Blot: Rpb1
IP: Gβ1–4
Blot: Gβ1–4
Total Lysate
Blot: Rpb1
Total Lysate
Blot: Gβ1–4
F
Ratio of RNA Pol II immunoprecipitated with Gβ1-4 (fold change over control)
2.5
2.0
1.5
1.0
0.5
0.0
DMSO / DMEM
DMSO / AngII
Importazole/ DMEM
Importazole / AngII

Figure 2.

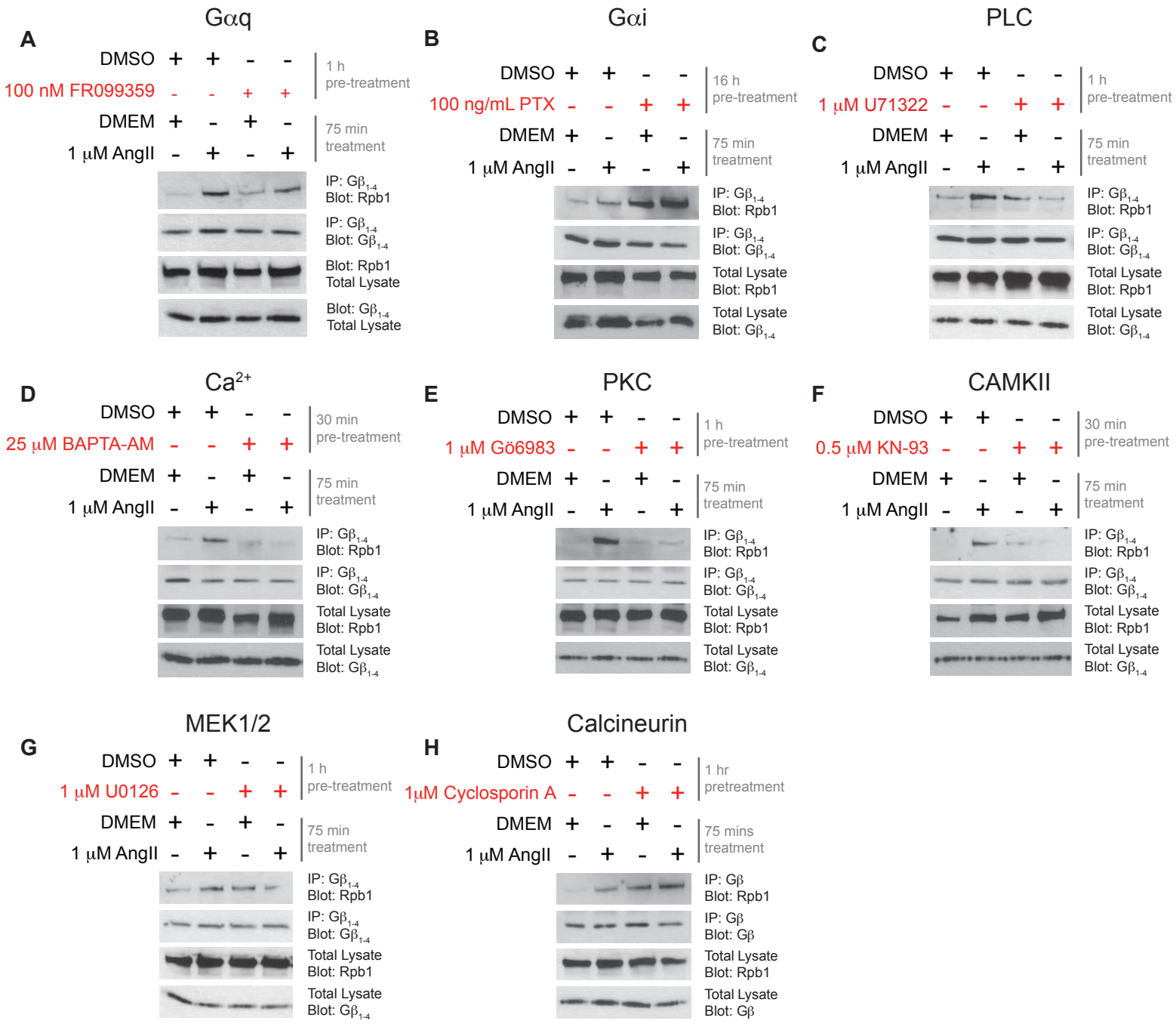
A
Gαq
DMSO + + - -
100 nM FR099359 - - + +
1 h pre-treatment
DMEM + - + -
1 μM AngII - + - +
75 min treatment
IP: Gβ1-4 Blot: Rpb1
IP: Gβ1-4 Blot: Gβ1-4
Blot: Rpb1 Total Lysate
Blot: Gβ1-4 Total Lysate
B
Gαi
DMSO + + - -
100 ng/mL PTX - - + +
16 h pre-treatment
DMEM + - + -
1 μM AngII - + - +
75 min treatment
IP: Gβ1-4 Blot: Rpb1
IP: Gβ1-4 Blot: Gβ1-4
Total Lysate Blot: Rpb1
Total Lysate Blot: Gβ1-4
C
PLC
DMSO + + - -
1 μM U71322 - - + +
1 h pre-treatment
DMEM + - + -
1 μM AngII - + - +
75 min treatment
IP: Gβ1-4 Blot: Rpb1
IP: Gβ1-4 Blot: Gβ1-4
Total Lysate Blot: Rpb1
Total Lysate Blot: Gβ1-4
D
Ca2+
DMSO + + - -
25 μM BAPTA-AM - - + +
30 min pre-treatment
DMEM + - + -
1 μM AngII - + - +
75 min treatment
IP: Gβ1-4 Blot: Rpb1
IP: Gβ1-4 Blot: Gβ1-4
Total Lysate Blot: Rpb1
Total Lysate Blot: Gβ1-4
E
PKC
DMSO + + - -
1 μM Gö6983 - - + +
1 h pre-treatment
DMEM + - + -
1 μM AngII - + - +
75 min treatment
IP: Gβ1-4 Blot: Rpb1
IP: Gβ1-4 Blot: Gβ1-4
Total Lysate Blot: Rpb1
Total Lysate Blot: Gβ1-4
F
CAMKII
DMSO + + - -
0.5 μM KN-93 - - + +
30 min pre-treatment
DMEM + - + -
1 μM AngII - + - +
75 min treatment
IP: Gβ1-4 Blot: Rpb1
IP: Gβ1-4 Blot: Gβ1-4
Total Lysate Blot: Rpb1
Total Lysate Blot: Gβ1-4
G
MEK1/2
DMSO + + - -
1 μM U0126 - - + +
1 h pre-treatment
DMEM + - + -
1 μM AngII - + - +
75 min treatment
IP: Gβ1-4 Blot: Rpb1
IP: Gβ1-4 Blot: Gβ1-4
Total Lysate Blot: Rpb1
Total Lysate Blot: Gβ1-4
H
Calcineurin
DMSO + + - -
1μM Cyclosporin A - - + +
1 hr pretreatment
DMEM + - + -
1 μM AngII - + - +
75 mins treatment
IP: Gβ Blot: Rpb1
IP: Gβ Blot: Gβ
Total Lysate Blot: Rpb1
Total Lysate Blot: Gβ

Figure 3.

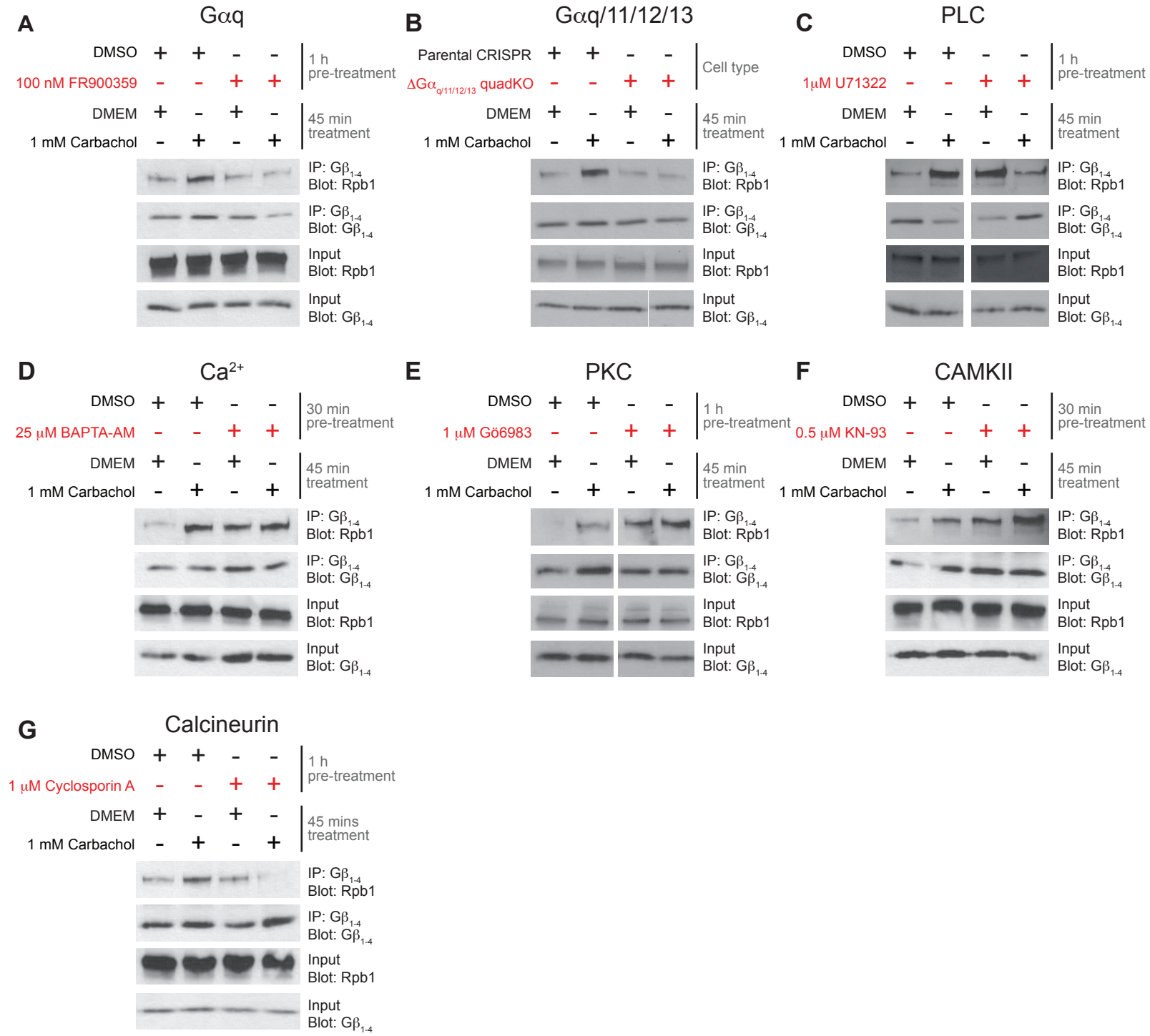
A
Gαq
DMSO + + - -
100 nM FR900359 - - + +
1 h pre-treatment
DMEM + - + -
1 mM Carbachol - + - +
45 min treatment
IP: Gβ1-4 Blot: Rpb1
IP: Gβ1-4 Blot: Gβ1-4
Input Blot: Rpb1
Input Blot: Gβ1-4
B
Gαq/11/12/13
Parental CRISPR + + - -
ΔGαq/11/12/13 quadKO - - + +
Cell type
DMEM + - + -
1 mM Carbachol - + - +
45 min treatment
IP: Gβ1-4 Blot: Rpb1
IP: Gβ1-4 Blot: Gβ1-4
Input Blot: Rpb1
Input Blot: Gβ1-4
C
PLC
DMSO + + - -
1μM U71322 - - + +
1 h pre-treatment
DMEM + - + -
1 mM Carbachol - + - +
45 min treatment
IP: Gβ1-4 Blot: Rpb1
IP: Gβ1-4 Blot: Gβ1-4
Input Blot: Rpb1
Input Blot: Gβ1-4
D
Ca2+
DMSO + + - -
25 μM BAPTA-AM - - + +
30 min pre-treatment
DMEM + - + -
1 mM Carbachol - + - +
45 min treatment
IP: Gβ1-4 Blot: Rpb1
IP: Gβ1-4 Blot: Gβ1-4
Input Blot: Rpb1
Input Blot: Gβ1-4
E
PKC
DMSO + + - -
1 μM Gö6983 - - + +
1 h pre-treatment
DMEM + - + -
1 mM Carbachol - + - +
45 min treatment
IP: Gβ1-4 Blot: Rpb1
IP: Gβ1-4 Blot: Gβ1-4
Input Blot: Rpb1
Input Blot: Gβ1-4
F
CAMKII
DMSO + + - -
0.5 μM KN-93 - - + +
30 min pre-treatment
DMEM + - + -
1 mM Carbachol - + - +
45 min treatment
IP: Gβ1-4 Blot: Rpb1
IP: Gβ1-4 Blot: Gβ1-4
Input Blot: Rpb1
Input Blot: Gβ1-4
G
Calcineurin
DMSO + + - -
1 μM Cyclosporin A - - + +
1 h pre-treatment
DMEM + - + -
1 mM Carbachol - + - +
45 mins treatment
IP: Gβ1-4 Blot: Rpb1
IP: Gβ1-4 Blot: Gβ1-4
Input Blot: Rpb1
Input Blot: Gβ1-4

Figure 4.

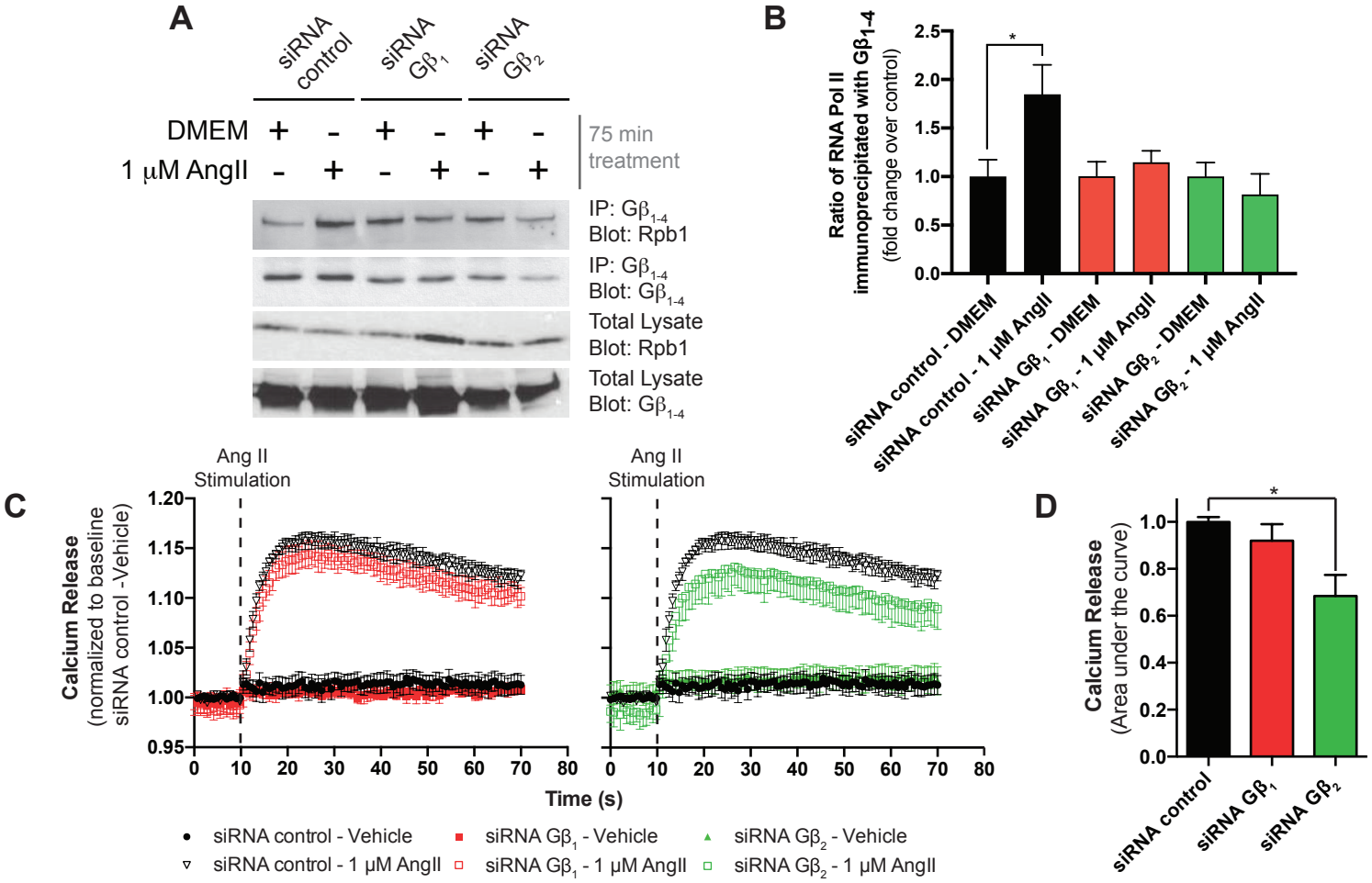
A
siRNA control
siRNA Gβ1
siRNA Gβ2
DMEM + - + - + -
1 μM AngII - + - + - +
75 min treatment
IP: Gβ1-4 Blot: Rpb1
IP: Gβ1-4 Blot: Gβ1-4
Total Lysate Blot: Rpb1
Total Lysate Blot: Gβ1-4
B
Ratio of RNA Pol II immunoprecipitated with Gβ1-4 (fold change over control)
siRNA control - DMEM
siRNA control - 1 μM AngII
siRNA Gβ1 - DMEM
siRNA Gβ1 - 1 μM AngII
siRNA Gβ2 - DMEM
siRNA Gβ2 - 1 μM AngII
C
Ang II Stimulation
Calcium Release (normalized to baseline siRNA control -Vehicle)
Time (s)
siRNA control - Vehicle
siRNA control - 1 μM AngII
siRNA Gβ1 - Vehicle
siRNA Gβ1 - 1 μM AngII
siRNA Gβ2 - Vehicle
siRNA Gβ2 - 1 μM AngII
D
Calcium Release (Area under the curve)
siRNA control
siRNA Gβ1
siRNA Gβ2

Figure 5.

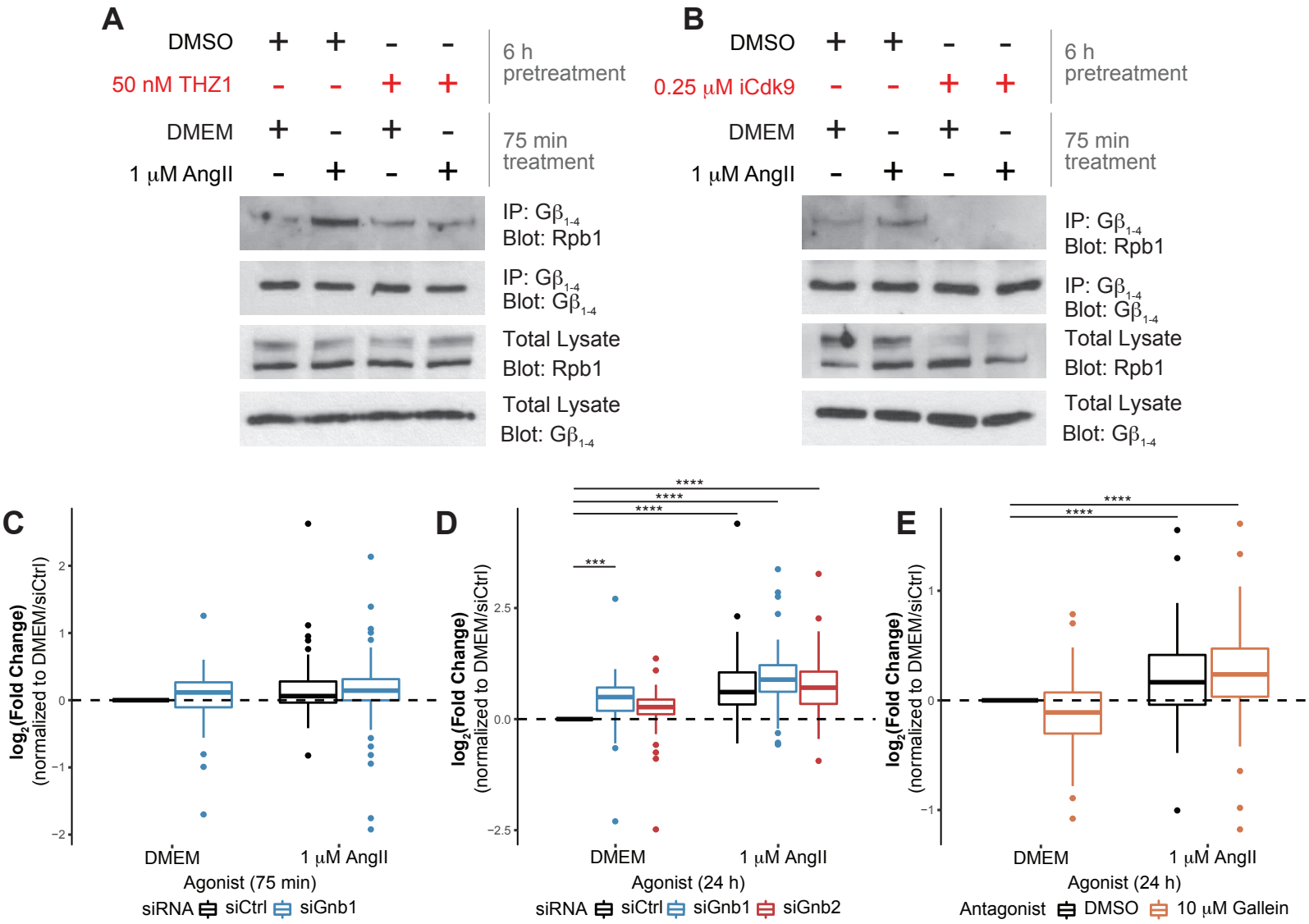
A
DMSO + + - -
50 nM THZ1 - - + +
6 h pretreatment
DMEM + - + -
1 μM AngII - + - +
75 min treatment
IP: Gβ1-4
Blot: Rpb1
IP: Gβ1-4
Blot: Gβ1-4
Total Lysate
Blot: Rpb1
Total Lysate
Blot: Gβ1-4
B
DMSO + + - -
0.25 μM iCdk9 - - + +
6 h pretreatment
DMEM + - + -
1 μM AngII - + - +
75 min treatment
IP: Gβ1-4
Blot: Rpb1
IP: Gβ1-4
Blot: Gβ1-4
Total Lysate
Blot: Rpb1
Total Lysate
Blot: Gβ1-4
C
log2(Fold Change)
(normalized to DMEM/siCtrl)
DMEM
1 μM AngII
Agonist (75 min)
siRNA siCtrl siGnb1
D
****
****
****
***
log2(Fold Change)
(normalized to DMEM/siCtrl)
DMEM
1 μM AngII
Agonist (24 h)
siRNA siCtrl siGnb1 siGnb2
E
****
****
log2(Fold Change)
(normalized to DMEM/siCtrl)
DMEM
1 μM AngII
Agonist (24 h)
Antagonist DMSO 10 μM Gallein

Figure 6.

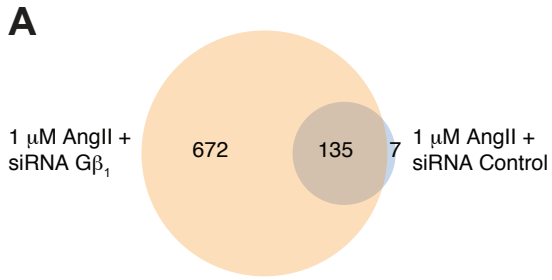

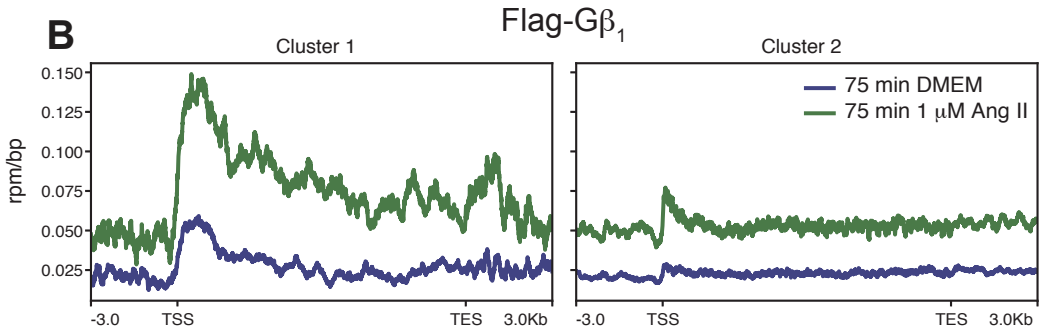

D

GO ID	Term	p-value
GO:0071356	cellular response to tumor necrosis factor	3.3E-10
GO:0071347	cellular response to interleukin-1	6.2E-08
GO:0043065	positive regulation of apoptotic process	5.1E-08
GO:0044344	cellular response to fibroblast growth factor	2.2E-08

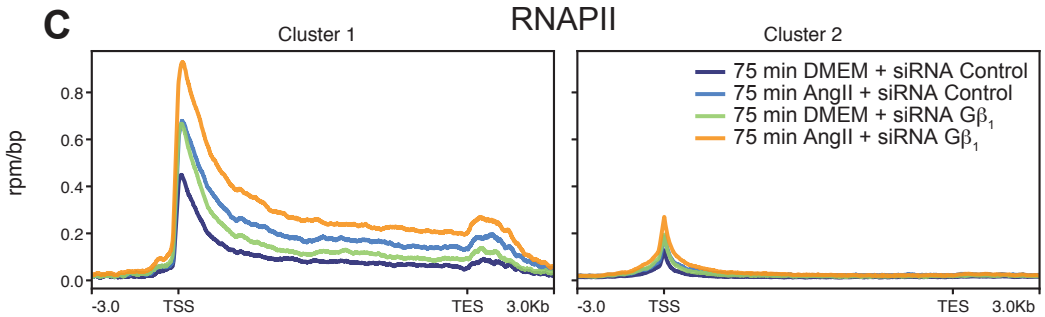

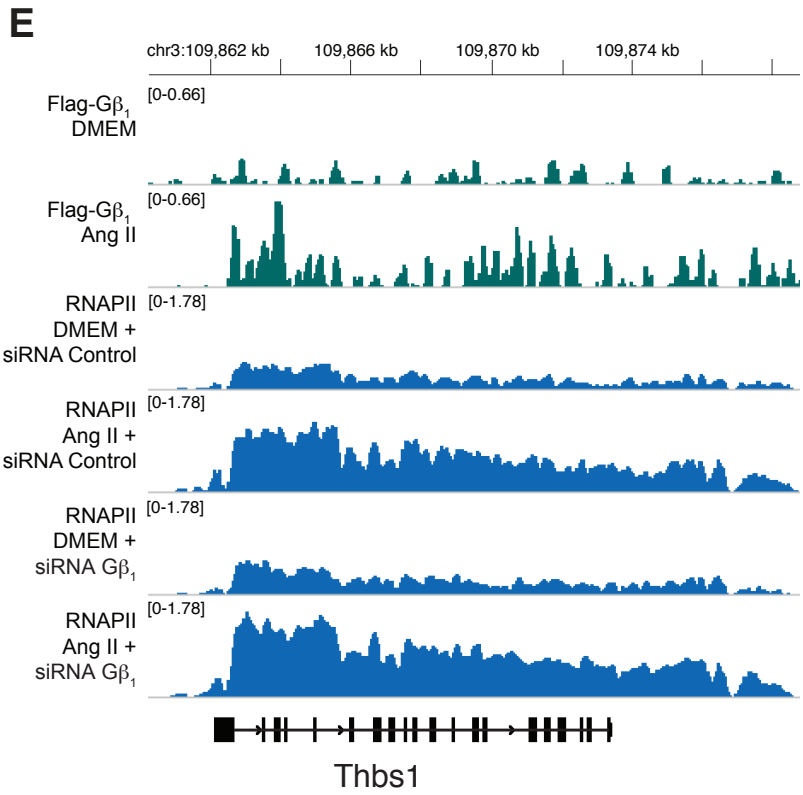

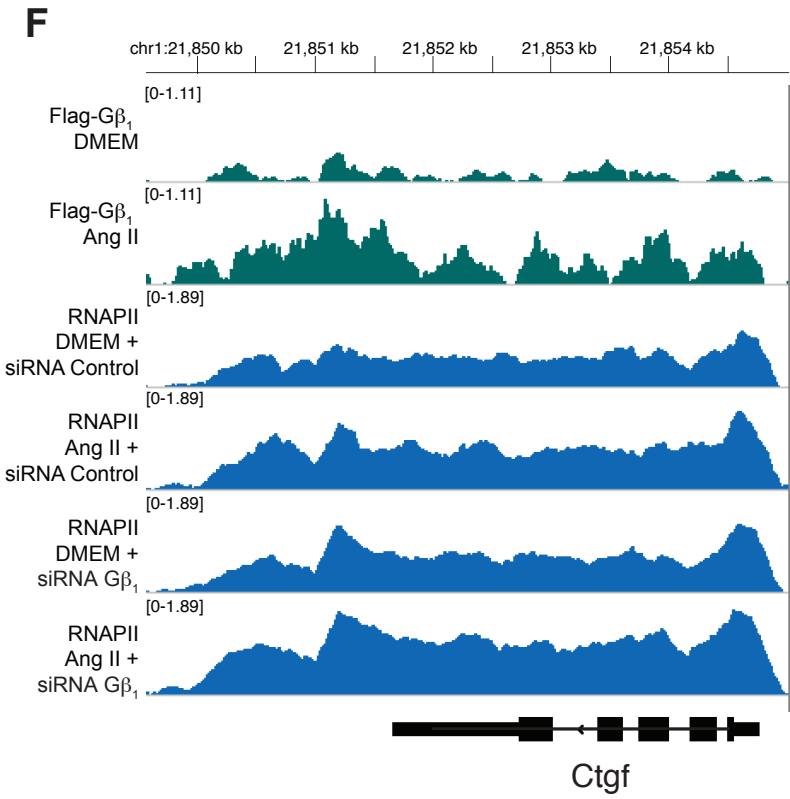

Supplemental Figure 1.

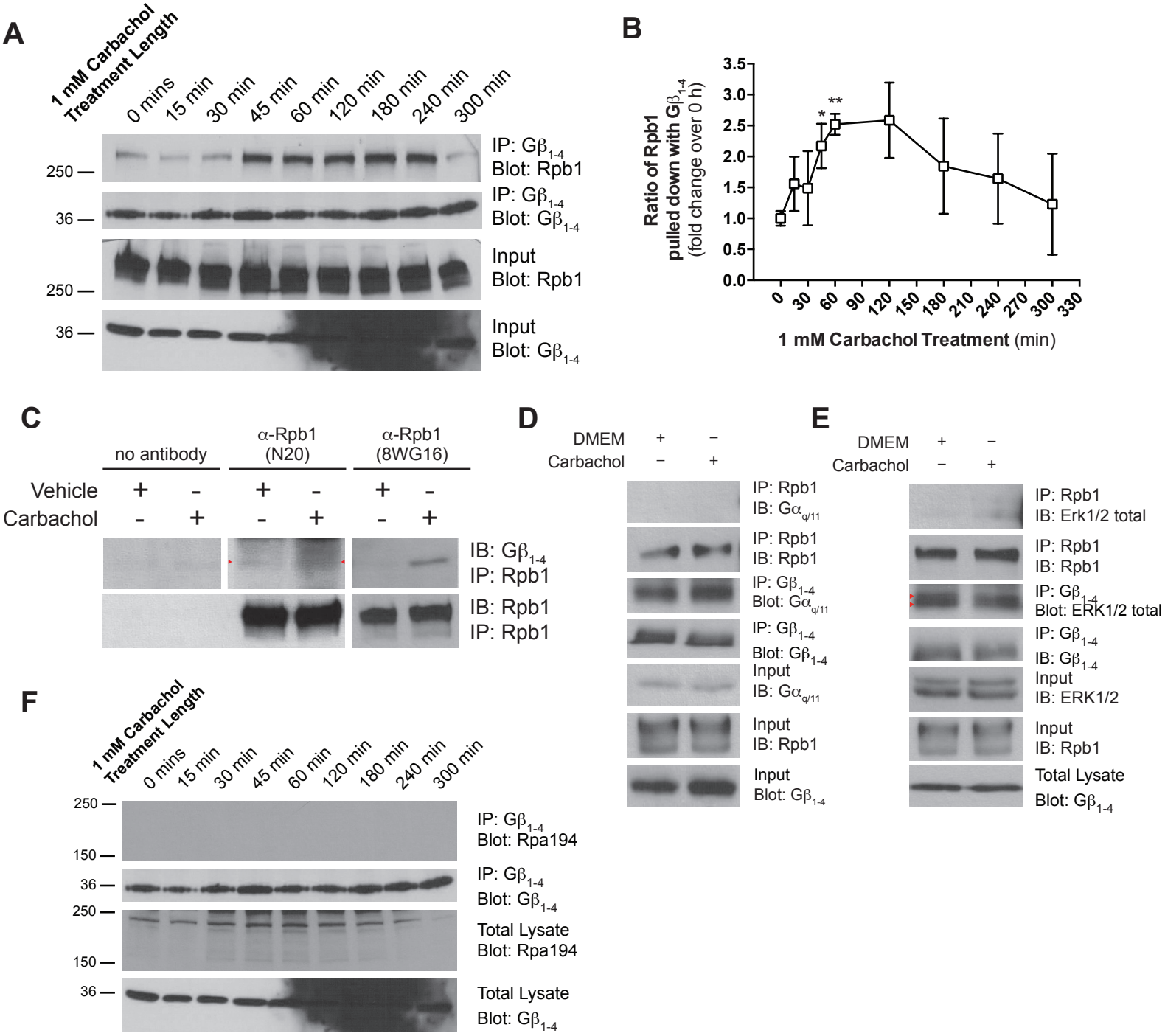

Supplmental Figure 2.

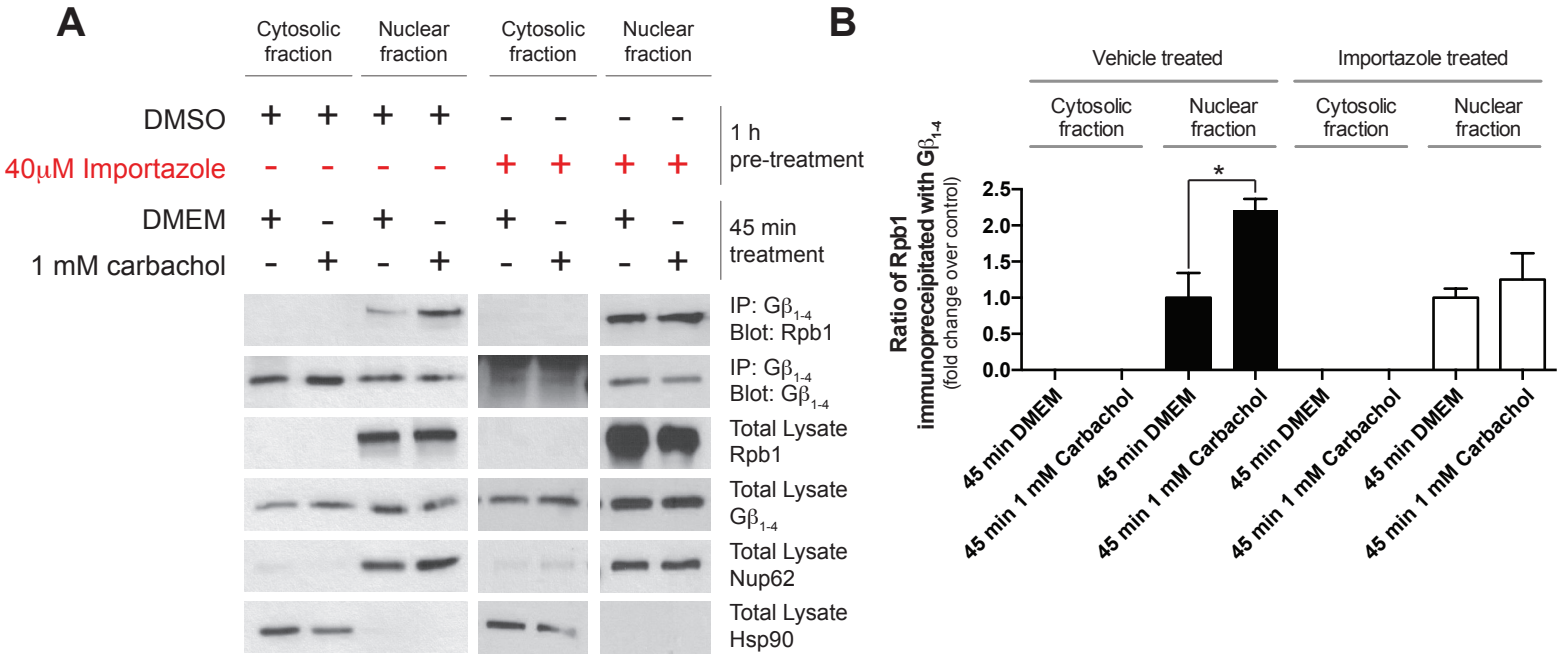

Supplemental Figure 3

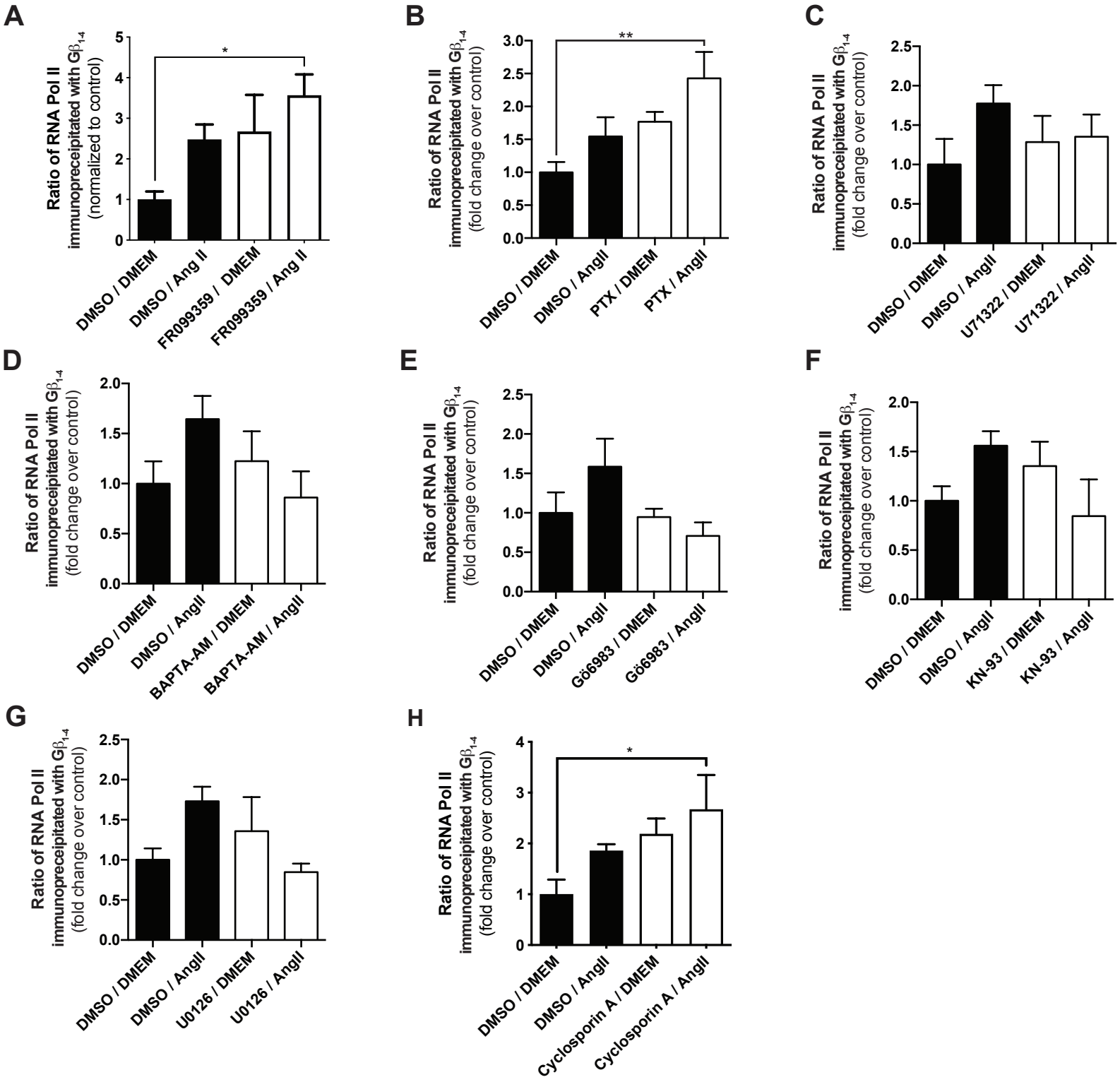

Supplemental Figure 4

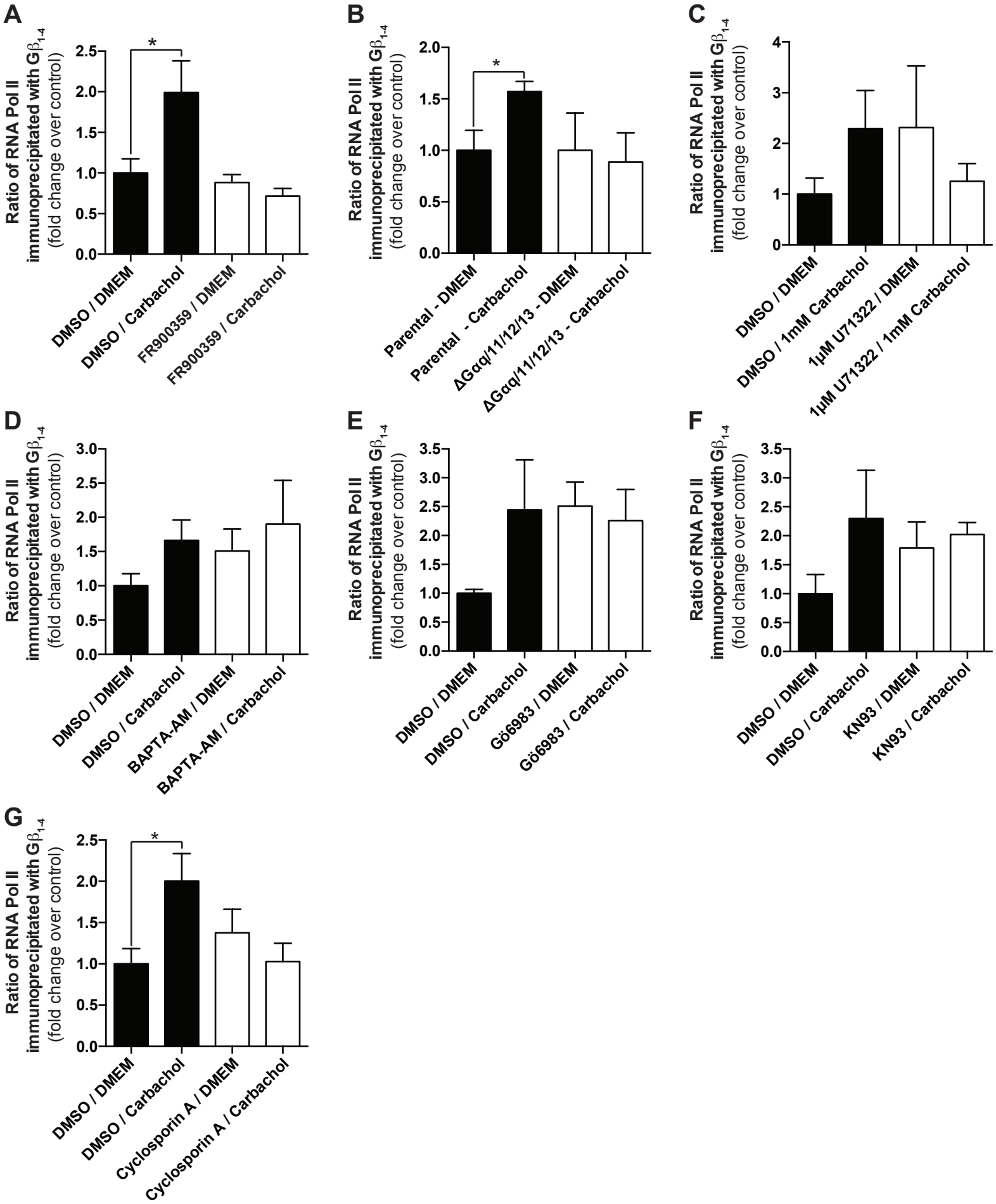

Supplemental Figure 5

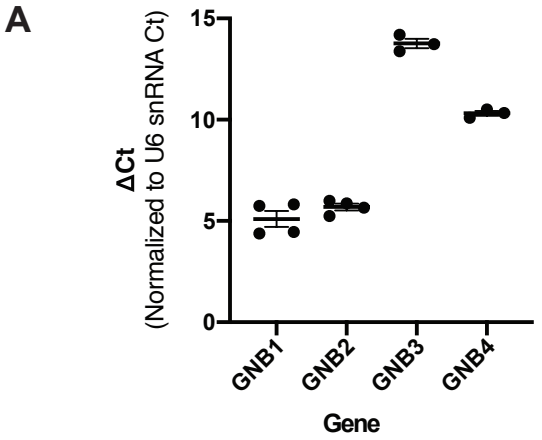

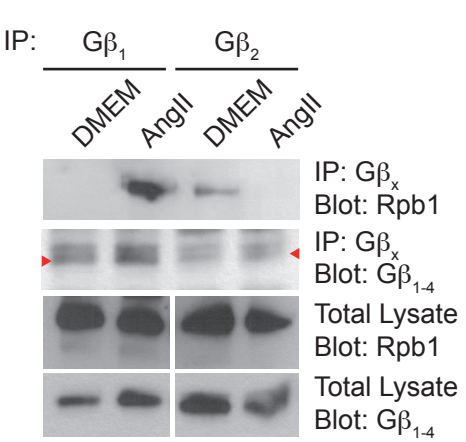

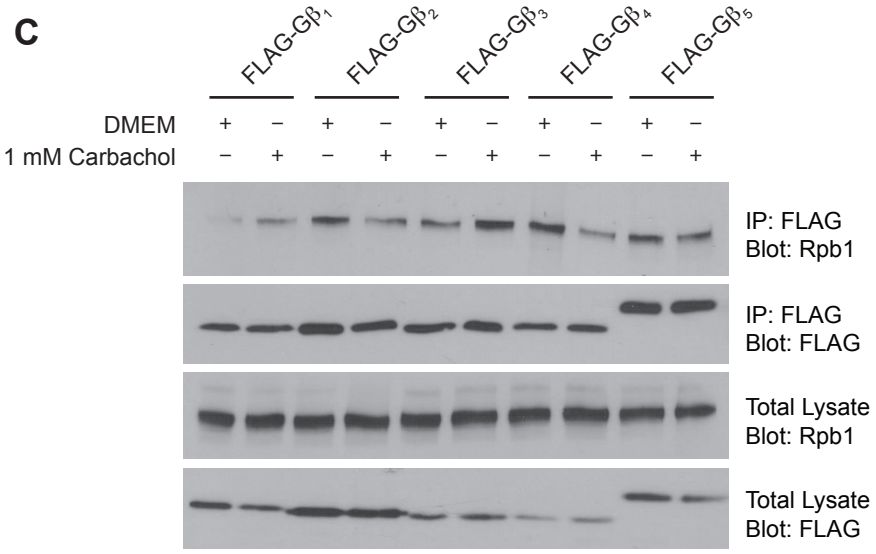

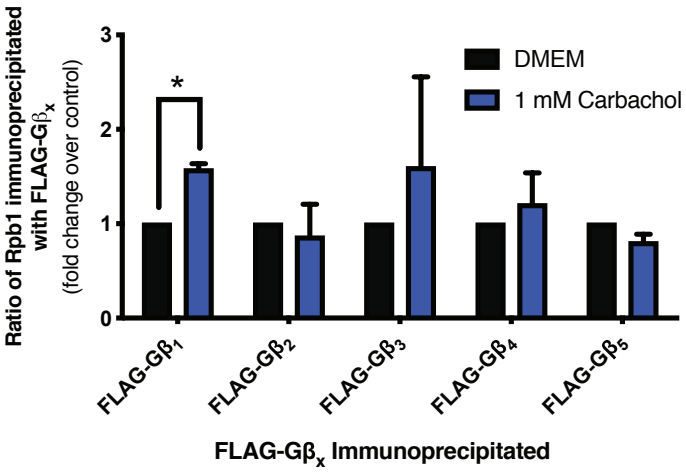

Supplemental Figure 6

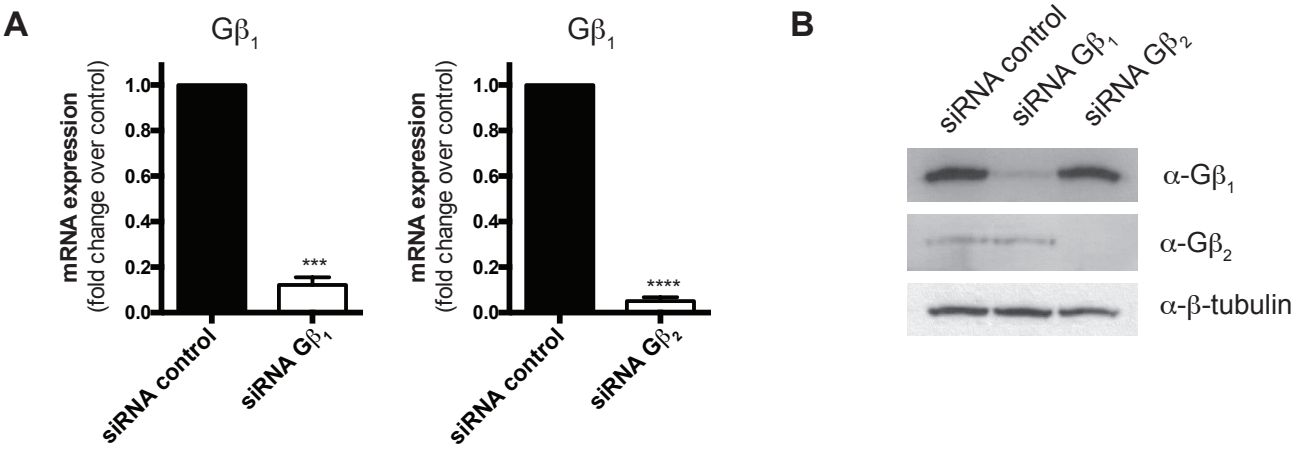

Supplemental Figure 7

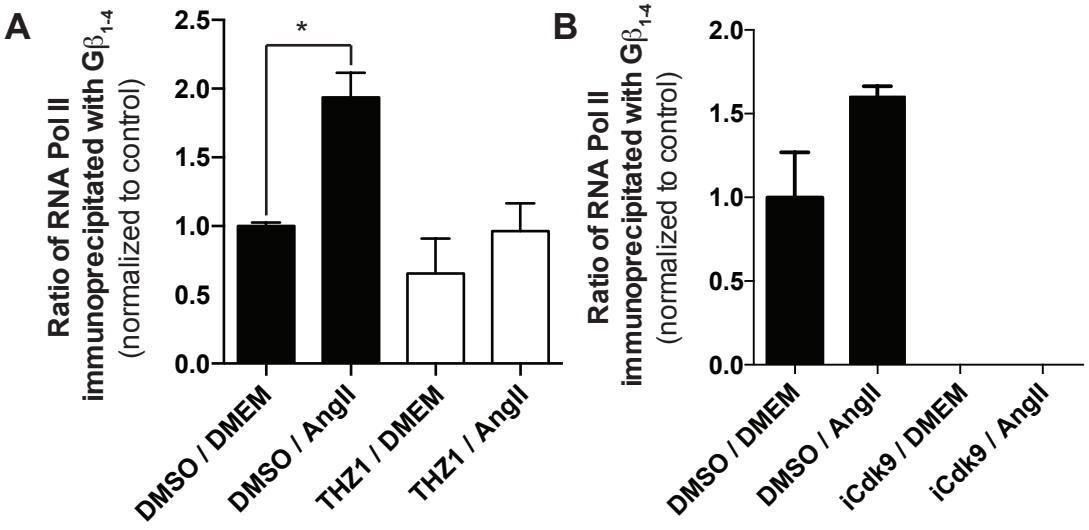

Supplemental Figure 8

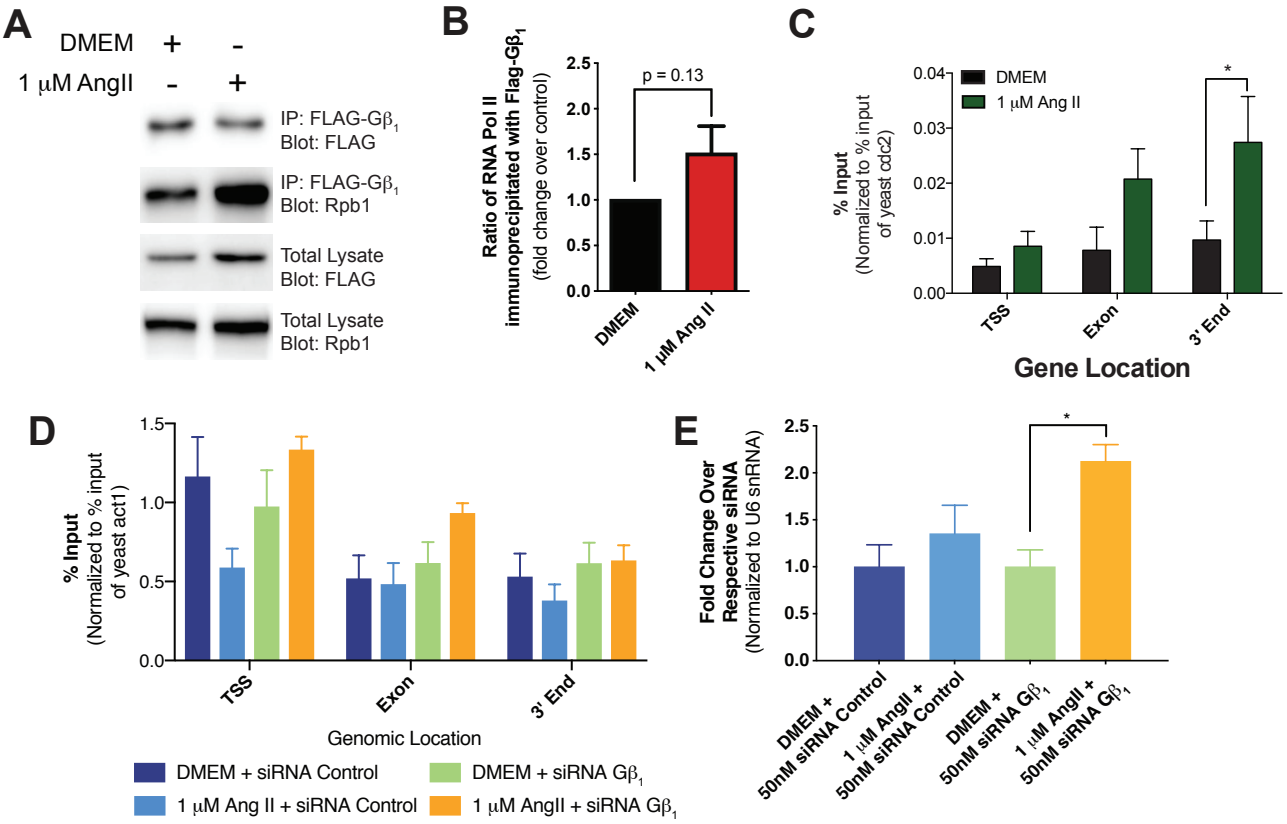
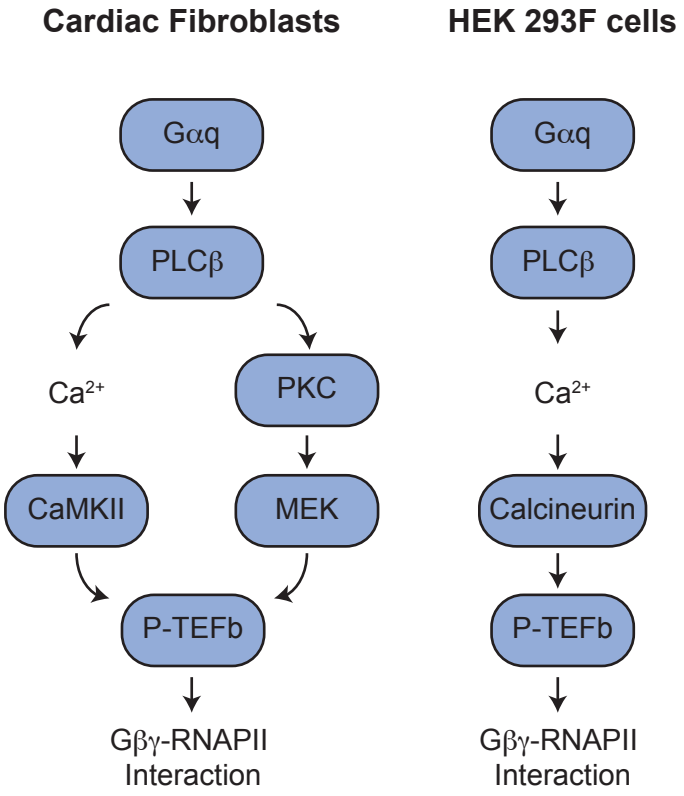
Supplemental Figure 9